UNIVERSITÀ DI PADOVA

Dipartimento di Ingegneria dell'Informazione

Scuola di Dottorato in Ingegneria dell'Informazione

Indirizzo in Scienza e Tecnologia dell'Informazione

XXVII Ciclo

Internet of things and vehicles in the context of 5G

Ph.D. school Director: Chiar.^{mo} Prof. Matteo Bertocco

Course Director: Chiar.^{mo} Prof. Carlo Ferrari

Supervisor: Chiar.^{mo} Prof. Lorenzo Vangelista

Ph.D. candidate: Giulio Ministeri

To my dears
and those who made this possible.

Abstract

In these years we are experiencing an incredible explosion for mobile connectivity. Devices such as smart-phones, tablets and laptops are more and more data hungry, asking for faster and faster connections. In the meantime, many industry sectors are pushing mobile network operators to provide internet connectivity with different characteristics for a new set of machine-driven applications. Machine-to-machine (M2M) or machine type communications (MTC), is the new paradigm: lower latencies, lower energy consumption, less signalling, higher reliability, are only few of new requirements. MTC devices will become a massive presence in tomorrow mobile networks and finally the Internet of Things will become real in its entirety.

Although still under constant update, the current 4G mobile networks have some limitations due to their intrinsic architecture.

A newer disruptive mobile network generation is the only possible solution to satisfy the future demands for connectivity. While within the so-called 5G networks, many new technologies are under study, focusing on reaching higher point-to-point data-rates, one of the most important aspects of 5G is the support for MTC.

In this thesis different aspects of M2M communications are taken into account.

Inter-vehicular communications and the IEEE 802.11p protocol for vehicular ad-hoc networks are analysed. In particular the IEEE 802.11p shortcomings on channel response estimation and channel access are taken into consideration. The physical layer of the IEEE 802.11p protocol does not provide sufficient information to track the channel response ; we propose a novel technique that exploits information provided by in-car sensors like GPS or speedometer to improve channel response tracking. Current protocols for vehicular direct communications considers the concurrent use of more than one radio channel at the same time, and leave to terminals

the duty of choosing which channel to use. In this thesis we consider the most common channel occupancy detectors, derived by the cognitive radio theory, in a vehicular environment, and measure their performances in terms of probability of misdetection and detection delay.

In the field of MTC, we present out implementation of an IETF IPv6-6LoWPAN protocol stack for resource-constrained devices. The stack provides the minimum requirements for these devices to support IPv6-based connectivity. The architecture is organized to decouple the stack from the data-link protocol and to seamlessly manage more than one radio access technology interface present in the device. Our tests show an increase in the final throughput respect to the other most known implementation, thanks to a memory usage optimization.

Finally 5G networks and green communications are considered in this thesis. In particular we analyse HARQ protocols, largely used in modern wireless protocols, in terms of energy efficiency. We use the recent theory on channel coding in finite block-length regime by Polyanskiy-Poor-Verdú, the most appropriate in MTC scenarios, as starting point to find the analytic formula of the outage probability for HARQ protocols of Type-I and Type-II. We then propose a novel optimal allocation strategy for the transmitting power of the subsequent transmission attempts. Results show the outstanding performances in terms of energy saved that even the simplest combining techniques that such protocols use, could bring into play.

Sommario

Negli ultimi anni si sta assistendo ad un'esplosione nella domanda di connettività in mobilità. Dispositivi quali smart-phone, tablet e laptop offrono funzionalità e servizi sempre più basati sulla disponibilità di una connessione sempre attiva.
Allo stesso modo, sempre più settori dell'industria premono gli operatori di rete mobile, chiedendo connettività per una nuova classe di dispositivi che rientrano nella categoria del Machine-Type-Communication. Coi termini Machine- Type- Communication (MTC) o Machine-2-Machine (M2M) si indica un paradigma con il quale si identificano una pletora di nuovi servizi di connettività in cui vincoli sulla latenza, disponibilità. affidabilità, consumo energetico della connessione sono più stringenti e meglio definiti.
Le MTC diventeranno in un futuro prossimo una presenza massiva nelle reti cellulari, dando vita finalmente al mondo globalmente interconnesso descritto dal paradigma dell'Internet delle Cose.
Sebbene in costante evoluzione e aggiornamento l'attuale generazione di rete mobile 4G ha alcune limitazioni intrinseche che rendono necessario un ulteriore salto generazionale ad una rete 5G di nuova concezione, come unica soluzione percorribile per soddisfare la crescente domanda di connettività. Nonostante in letteratura la maggior parte delle nuove soluzioni tecnologiche proposte hanno come obiettivo il raggiungimento di connessioni più veloci, uno degli aspetti più importanti del 5G è il pieno supporto alle MTC.
In questa tesi vengono presi in esame alcuni aspetti delle comunicazioni M2M. In primo luogo si prendono in considerazione le reti veicolari, nello specifico si affrontano alcune criticità dell'attuale protocollo per reti wireless ad-hoc tra veicoli, il protocollo IEEE 802.11p, per ciò che riguarda la stima del canale radio e il meccanismo di accesso al mezzo. Il livello fisico del protocollo non fornisce sufficienti

risorse per permettere il tracking delle fluttuazioni del canale radio, qui proponiamo una tecnica innovativa che sfrutta informazioni aggiuntive provenienti da sensori e sistemi elettronici, di cui le moderne auto sono dotate, per migliorare il tracking del canale radio.

Gli attuali protocolli per le reti veicolari prevedono l'uso concorrente di più canali radio, e lasciano totale libertà ai terminali sui metodi di scelta del canale radio da utilizzare. In questo lavoro, vengono presi in esame alcuni tra i più comuni rilevatori di occupazione del canale radio, mutuati dalla teoria del "cognitive radio", e ne vengono analizzate le performance in termini di probabilità di mancata rilevazione e ritardo di rilevazione in ambiente veicolare.

Nel campo delle MTC, presentiamo l'implementazione di uno stack protocollare IETF IPv6-6LoWPAN, realizzato per permettere a dispositivi low-cost con risorse limitate, di supportare comunicazioni su rete IPv6. L'architettura dello stack stata progettata allo scopo di disaccoppiare le funzionalità dello stack dal particolare protocollo data-link utilizzato, e di supportare dispositivi equipaggiati con più moduli per la comunicazione wireless. I test comparativi dimostrano un throughput maggiore rispetto all'implementazione più conosciuta del protocollo IPv6 per questi dispositivi.

In conclusione, sono messi in relazione le reti 5G e il paradigma delle green communication . I protocolli di tipo Automatic Repeat reQuest (ARQ) ibrido, largamente usati nelle moderne reti cellulari, vengono analizzati in termini di efficienza energetica usando i recenti risultati di Polyanskiy-Poor-Verdú sulla capacità di canale in regime di parola di codice di lunghezza finita. Tale teoria affronta l'analisi della capacità di correzione dei codici di canale a fronte di una parola di codice di lunghezza finita, teoria che si concilia con la natura delle reti MTC.

L'analisi propone inoltre, una tecnica di ottimizzazione della potenza trasmissiva nelle ritrasmissioni dei protocolli HARQ di tipo Type-I e Type-II. L'analisi mostra i risultati ottenuti in termini di probabilità di outage finale e di risparmio energetico ottenuto.

Contents

Chapter 1

Introduction

In the next five years we will experience an explosion of wireless and mobile communications. According to the estimations of the future mobile traffic demand [1], [2], in 2020 mobile networks will have to provide at least 1000 times the capacity that current commercially available cellular systems are providing.
In parallel to this growth, there is a strong drive from many industry sectors in exploiting the benefit of wireless internet connectivity to finally enable the paradigm of Internet of Things (IoT) in its entirety. Finally smart metering, smart monitoring, smart sensing and, more generally, smart cities and smart grids can become reality; e-health, e-commerce will be fully supported; autonomous production lines and autonomous transportation systems will be deployed.
These new devices are not human-driven but machine-driven and, current forecasts, predict that they will be massively deployed for a wide range of fields for a final count of about 25 billions of connected terminals in 2020 (Fig. 1.2). This new class of devices asks for a completely different connectivity requirements, defined by the terms Machine-to-Machine (M2M) or Machine-Type-Communication (MTC).
The growing request of connectivity from human-centric devices and the appearance of MTC impose very challenging goals for the future mobile networks. Human users are asking for data-rates in the order of ten Gbit/s, coming applications like augmented or virtual reality need maximum latency of 1 to 3 ms in order to not to incur in cyber sickness [3], MTC devices point out different needs for their connectivity profile: low-power devices (e.g. for smart metering) prefer very simple radio access technologies and protocols in order to save energy and last longer; sensors for

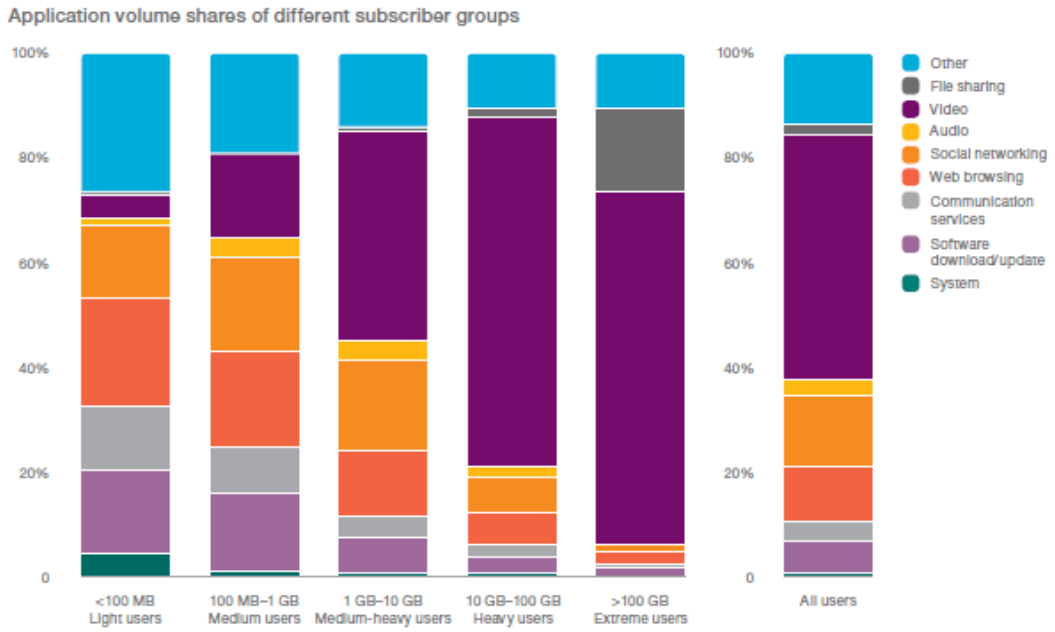

Figure 1.1. *traffic volume for different applications, source [1]*

industrial controlling require reliability to guarantee connectivity and reachability in every conditions and every moment; devices for vehicular communications and traffic safety ask for low latency for preventing accident and fatalities; the massive deployments of connected terminals have not to congest the network and threaten its integrity, and finally, all these requests need to be satisfied and coexist within the same network or even in the same device, sharing the same resources.

Although the current 4G technology is evolving and making significant effort to fulfil the growing requests for connectivity by mobile users and for the M2M by industries, it is a common belief that sooner or later this technology will be insufficient to support the growing connectivity demand due to the intrinsic limit of its architecture.

Mobile networks have always been designed with a cell-centric approach: downlink and uplink connections, control and data plane, signal processing are duties that have always been assigned to BSs uniformly. This axiom has started to fall apart, thank to new advances in wireless communication research, few shortcomings rose up.

4G, as previous generations network, has been designed with cell-centrism; even if latest 4G LTEs-A releases tried to include new wireless technologies, the fundamen-

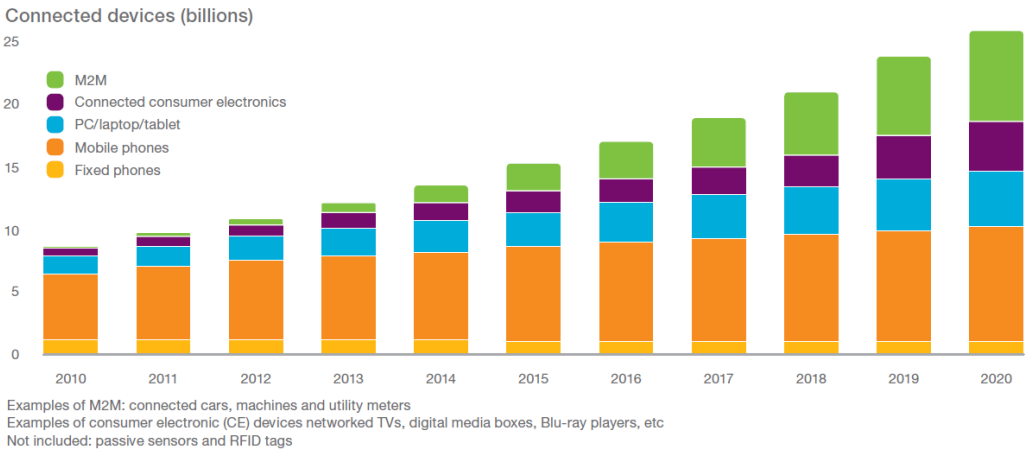

Figure 1.2. *forecast of the number of connected device till 2020, source [1]*

tal architecture does not natively support them, lowering the network densification and BSs with different capabilities could require a disruptive change in network architecture. As an example in [4] the idea of decoupling downlink and uplink connections has been proposed. The need for more spectrum calls for the adoption of new radio access technologies (RATs) able to cope with different propagation behaviours. In [5] phantom cell concept has been introduced where data plane and control plane has been split to both exploit reliability and speed of different RATs. The adoption of different RATs could be optimized by separating BS from its hardware. In [6] the cloud-RAN (radio access network) concept has been proposed: adjacent BSs share hardware resources located in a virtual machine able to dynamically reassign computation resources and reallocate them where most needed, with the advantage of having a centralized control of wireless resources (e.g. for inter-cell interference mitigation).

Hence, interest and discussions about next mobile network, so called 5G, have moved from being a merely academic researcher's intellectual exercise, to a full-fledged conversations among different stakeholders, researchers and engineers all over the world.

Projects, like METIS [7] and 5GNOW [8], have considered different aspects of 5G; industries have started to push international standardization institutions to create discussion and working groups to study the key enabling technologies; and international radio spectrum regulatory institutions have started to investigate possible solutions for spectrum allocation for 5G.

The approach for designing the 5G network is based on some key points summarized here:

- area capacity, i.e. the amount of data the network can handle measured as bits/s per unit area, will at least be 1000 times higher than 4G;
- end user data rate will have to grow from 10 to 100 times the current 4G capabilities;
- latency of 4G is in the order of 10-15 milliseconds, 5G should be able (when needed) to shrink these values to 1-3 milliseconds;
- costs (CAPEX/OPEX), energy consumption, and resource utilization of the 5G network should be extremely lower than today's system in order to allow networks to grow as much as requested by the market at acceptable cost and energy use;
- energy usage of the 5G terminals, measured as Joule/bit, has to decrease (at least) of the same factor of the end-user data rate growth, simply to not to reduce battery lifetime of terminals;
- 5G needs to be more versatile to support different connectivity requirements at the same time in the most efficient way for both the network and the user equipment;
- 5G needs to provide better scalability to support larger range of connected devices with different connectivity classes independently of the required datarates;
- 5G needs to provide a new operating mode defined as Ultra Reliable Communication (URC), referred as the ability to provide a certain level of connectivity (with well specified characteristics) almost 100 % of the time.

1.1 5G promising technologies

The need to design a new mobile network from scratch, open the doors to a series of proposals for the adoption of new technologies and network architectures which

aim at reaching the challenging goals of 5G networks. Most of them are still immature, and unresolved issues are still under study, but some disruptive technologies are acquiring more and more credibility and there is a broadly agreement that they will probably be adopted by next cellular generation.

1.1.1 millimeter Wave (mmWave)

The scarcity of spectrum at microwave frequencies, and the fact that spectral efficiency of microwave links is approaching its fundamental limits, have motivated academia and industry world to consider the option to put large amount of bandwidth into play, i.e. to go up in frequencies.
At millimiter waves, i.e., frequencies ranging from 3 to 300 Ghz, there is an enormous amount of unused spectrum. The main reason of this unchartered waters, lies on the fact that since now, millimeter waves have always been considered unsuitable for mobile communications due to its propagation characteristics: the fundamental law of path loss in free space which states that attenuation grows with the square of the carrier frequency, the experimented lower ability to travel through objects and obstacles (blockage), and the consistent absorption of mmWaves by water and oxygen especially in frequencies around 60 GHz have always stopped mmWave being used for wireless communications.
Recent studies and progresses in RF design fields, leads to the certainty that propagation of mmWaves is not an insurmountable challenge. Large adaptive antenna arrays can be used to maintain the antenna aperture constant and electrically steer the beam to point the receiving antenna. Very narrow beam-forming also contributes to reduce the overall network interference, making mmWave systems to operate in noise-limited conditions respect to current systems which often operate in interference-limited conditions.
Although already standardized in the IEEE802.11ad [9] and promising results in point-to-point links have been obtained [10] [11], mmWave has a list of open issues that are still under study.
Having fully digital beam-formers for large antenna arrays is extremely expensive, both in terms of realization and energy consumption; current semiconductor technology for high speed ADC and DAC does not provide sufficiently low energy

consumption level, and traditional microWave architecture where each antenna is driven by an DAC/ADC, seems to be infeasible.
Highly responsive algorithms for adapting beam-forming in mobility scenarios are required, in order to not to incur in unexpected disconnections. Lastly, link acquisition is one of the most challenging problem which includes MAC layer design issues: establishing the connection between UEs and BSs both for initial access and during handoff involve scanning all the possible directions with extremely energy and time consuming operations. Having beam-forming capabilities both at BS and UE sides, creates great opportunities to reach very high data-rates but at the same time has the drawback of the so-called deafness problem, i.e. where the two beams are misaligned and transmitter and receiver can't reach each other even if they are in perfect line-of-sight condition.

1.1.2 Ultra Dense Network

It is a common thought that mobile network cells will shrink more and more ending with final sizes in the order of tens of square meters. Since the birth of the first generation cellular network, cell sizes have always tended to reduce their coverage area, governed by the well proved approach[12] that smaller cells lead to higher spatial spectrum efficiency and hence an increase of the overall network capacity. Current 4G has also embraced this paradigm and pico and femto-cell are under deployment as specified in the latest LTE-A Releases.
Within 5G, the trend of reducing the coverage area of mobile cells by increasing the number of BSs per unit area will continue, getting to the so-called Ultra Dense Networks (UDNs).
Even though, theoretically cell shrinkage could benefit the average network throughput indefinitely, in reality, as BSs become more and more lightly loaded the effective cell-splitting gain decreases [13]. In fact as the cells shrink under a certain size, they start to compete for the same users becoming even more lightly loaded, and thus resulting in an unworthy densification.
UDN adds significant complexity in terms of mobility support; speaking of outdoor terminals, the always-on connectivity that users are expected to experience, becomes difficult in ultra dense networks, in particular, if paired with the adoption

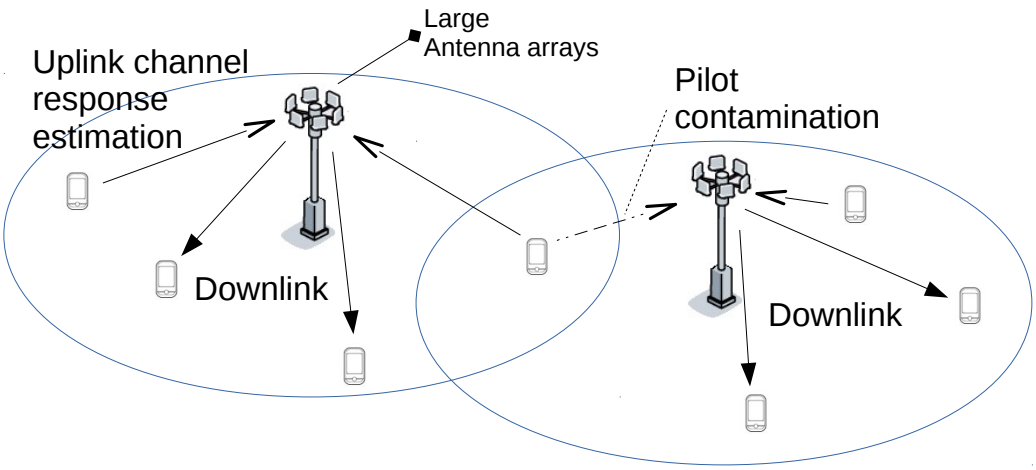

Figure 1.3. *Pilot contamination in massiveMIMO systems*

of mmWave technology, in UDN scenario, handover will be particularly challenging especially in very high mobility scenarios.
Last but surely not least, there are costs: building BSs with a coverage area comparable to that of traditional Wi-Fi networks, cannot be more expensive than consumer Wi-Fi APs. Mobile network operator' expenses for installation permissions, site rental fees, and maintenance costs does not scale along with the number of deployed BSs, so another economic model must be found. The proposals of transforming end-user Wi-Fi APs in femtocells BSs [12] could surely cut the costs of network densification, but poses some technical and legislative issues: end-user owned equipment can't be controlled by the operator, so some algorithms to self-reorganize the network are necessary, moreover to convince users to share their own equipment for the benefit of the network it is not straightforward, and in many countries, due to privacy laws it is not even legal.

1.1.3 massiveMIMO

MIMO (multiple input multiple output) systems are largely used in today wireless networks: last IEEE802.11 standards such as IEEE802.11n and IEEE802.11ac, and also 4G, make use of SU-MIMO (Single User MIMO).
Multi antenna systems take advantage of antenna diversity and spatial multiplexing to split an high rate data stream into different streams that can be transmitted

in parallel. In the best channel conditions, MIMO can increase the overall throughput by roughly a factor equals to the minimum number of available antennas at the transmitter and receiver.
The SU-MIMO, however, is limited by the number of antennas that can be fitted in the mobile device.
In massive MIMO, also known as large scale antenna system (LSAS), the higher freedom in designing and equipping BSs with large antenna arrays, is exploited: the number of transmitting antennas at the BS is greater than the sum of the antennas of the UEs. The BS has enough degrees of freedom to exploit the UEs' channel state information and jointly optimize the transmission power of each antenna, to concurrently transmit the UE downlink data streams. With this technique the number of achievable parallel data streams is now limited by the minimum between the BS antennas and the sum of the involved UEs antennas; the gain in spectral efficiency due to parallel serving a large number of UEs is remarkable.
While very promising, massive MIMO still present a number of research challenges. Channel estimation is the greatest of the problems when working with large antenna arrays especially if terminals are moving: imposing the channel estimates to have a limited coherence time (due to moving UEs), forces the system to periodically reassign pilot sequences to the users for uplink channel impulse response estimation procedure. Thus, since the number of orthogonal pilot sequences is finite, the reuse of the same sequences can cause pilot contaminations among adjacent BSs (Fig. 1.3).
There are also issues about coexistence with other technologies such as mmWave or UDN. If antenna arrays are used for mmWave beam-forming, they cannot be used for MIMO, so correct balance must be find in order to maximize efficiency and final throughput of the network.
The co-existence with Ultra Dense Networks shows frictions: UDNs deployments will be possible only by designing very small BSs which cannot be equipped with large antenna arrays reducing, therefore, the possibility of reaching massiveMIMO capabilities.

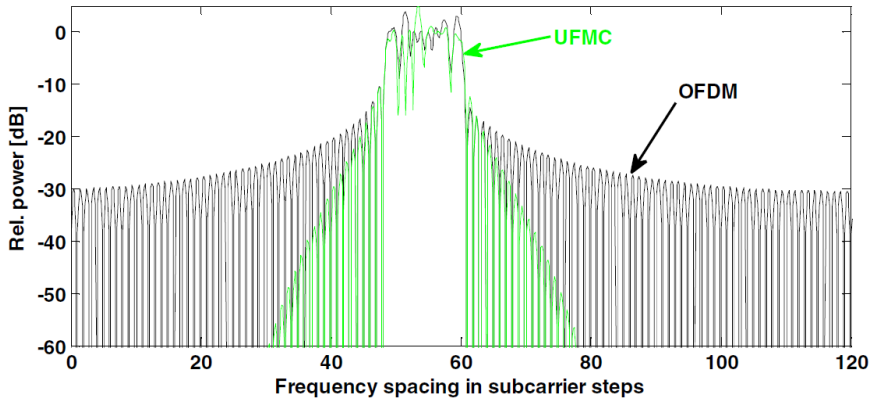

Figure 1.4. *UFMC and OFDM power spectral densities, UFMC side lobes are remarkably shorter than those of OFDM, [14]*

1.1.4 Waveform alternatives to OFDM

In the last years, OFDM signalling has taken the principal role in wired and wireless communications. Since its first applications (DSL) OFDM started growing its credibility as the best physical layer protocol for high-speed digital communications. OFDM qualities include:

- robust against frequency selective fading,
- outstanding efficiency thanks to FFT and iFFT algorithms,
- very simple equalization operations.

OFDM has also recently employed in multiple access environment. The OFDMA technique paired with TDMA, permits to create very fine-grained time-frequency grids where each small units of resources, named resource blocks, can be easily discriminated in the digital domain. 4G LTE standard currently adopts this combination of access algorithms to define its resource blocks. However OFDM has still unresolved issues like the high peak-to-average power ratio which forces transceivers to be equipped with high precision linear transceiver that typically lack on energy efficiency, the cyclic prefix and guard intervals that reduce the spectral efficiencym and the sensitivity to frequency synchronization and Doppler effects that compromise performances in a mobile environment.
Some new proposals for supporting both high-speed, and also low-speed low-power connections are growing in interests.

Faster-than-Nyquist signalling could overcome the problem of strict orthogonality and cyclic prefix [15] [16]. Filterbank multicarrier (FBMC) is a good candidate for asynchronous multiple access and fragmented spectrum communications [17]. Universal filtered multicarrier (UFMC) has been shown to improve efficiency by shrinking OFDM sidelobs (Fig. 1.4), and shows also good performance (respect to OFDM) in multiple access scenarios [18]. There are also proposals for maintaining OFDM as principal waveform to exploit acquired knowledge on OFDM waveform, but to modify the classical approach where OFDM parameters are fixed and designed to fit the worst-case scenario, and to make some of them dynamically tunable giving transceiver the ability to adapt wireless waveform to channel or network conditions [19].

1.1.5 Full Duplex Radio

Full duplex radio (FDR) technology enables devices to transmit and receive data simultaneously in the same frequency band, doubling the network throughput and the spectral efficiency, and also lower the average latency. Many researchers think that full duplex transceivers will be part of 5G systems, since recent advances in self-interference cancellation has shown that by using particular antenna placement and orthogonal polarizations techniques, up to 90 dB of attenuation of the self-interfered signal can be obtained [20]. Moreover FDR dramatically improves network efficiency in contention based networks since the hidden node problem almost disappears: while receiving a packet the node can transmit a simple beacon message, alerting the hidden nodes that a communication is occurring and that the channel is busy [21]. It also enhances the efficiency of relay nodes, by almost simultaneously retransmitting messages to destination, multi-hop link latency will drastically decreases [22].
However, this technology is still immature, there is no real-life application actually using full-duplex communications that could push FDR to be adopted in future 5G standards. Studies have only focused on a single-cell scenario, with one BS (or AP) and many terminals and no analysis has been made in a multi-cell scenario where interference management become more complex. FDR system leads to a completely

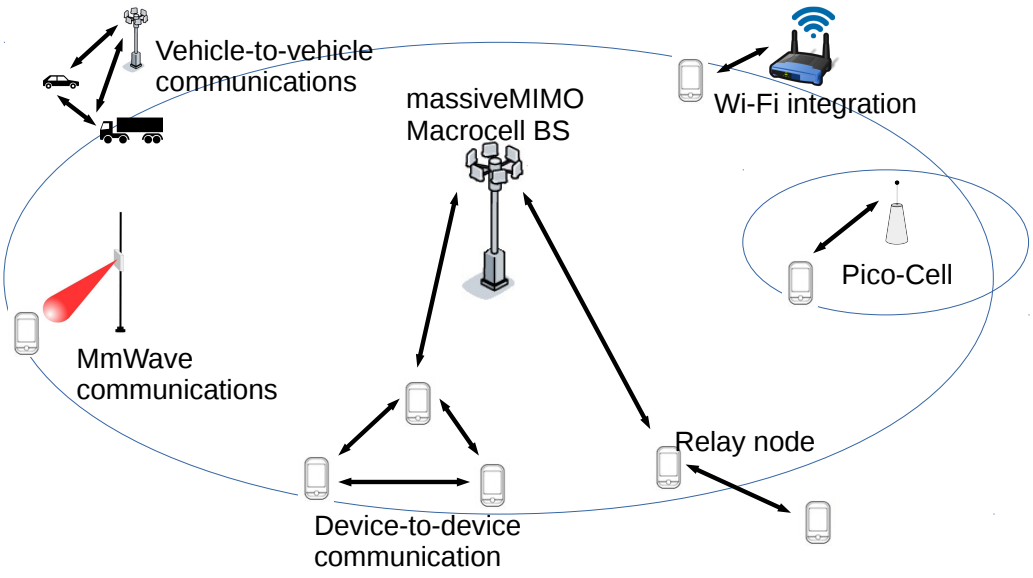

Figure 1.5. *5G scenario, devices must be able to communicate with many different Radio access technologies*

new set of scenarios where inter-cell an intra-cell interference takes new forms respect to current half-duplex wireless network, calling for new mitigation algorithms.

1.1.6 Heterogeneous networks and multi RAT system

Future mobile networks will continue the trend of embracing different RAT protocols and move towards what is named heterogeneous network. The key feature here is the integration of many different Radio Access technologies (RATs) within the terminal. 5G devices will very likely be equipped with a 2G, 3G, 4G, and 5G modems, and, as smart-phones currently do, they will also be capable of communicating using Wi-Fi standards. The difference with today smart-phones is that within 5G, there will be the integration of all these technology in one single aggregated interface. MultiRAT modems will be able to transparently and quickly switch from one RAT to another, arranging the decision based on both connection necessities (mobility, connection speed and latency) and network available resources. In fact the main difference from the current and past mobile networks will be the move toward a proactive management of connectivity, mobility and interference instead of simply reacting to changes of channel and/or network conditions; made possible

by algorithms that crossing all the layers, will make predictions based on device and application contexts.
5G will also support slow-rate RATs like Bluetooth, ZigBee and 6LoWPAN, used for communications of sensors and wearable devices, to not force MTC devices to be equipped with very expensive high-speed and energy greedy 5G modems.
Clearly, as for UDNs, multi-RAT networks will require novel interference mitigation and coordination techniques, together with faster and more reactive algorithms for managing handover. Cell association algorithms in core network systems will continuously optimize utility functions that express the instantaneous load of the BSs, the quality of experience level and connection requirements for the current applications of all the connected terminals, constantly looking for the best resources assignment that best exploit the available resources [23] [24] [25].
Also microelectronics technology should make a step forward to integrate different RAT technology, in one versatile and energy efficient modem, capable of operating in a wide range of frequencies and able to move from one RAT to another quickly, and efficiently.

1.1.7 Device to Device communications

As devices become smarter and smarter, they can play a more important role and start to actively contribute within the network for the sake of the network itself.
The most promising opportunity is the device-to-device D2D communications where terminals act not only as leafs node at the edges of the networks but as inner nodes; D2D goes beyond the concept of relay nodes, it envisions terminals as network peers able of establishing connections and/or exchanging data without the intervention of any supervisor node.
D2D objectives are few:

- to offload the network when communications are occurring between adjacent nodes in cases like content sharing or online gaming, or in MTC applications like car-to-car communications or wireless sensor networks.
- to increase network coverage by working as relay nodes to reach core network, or in cases where core network connection is not necessary to fulfil the application duties (Vehicle to vehicle communications)

- to reduce interference by lowering the in-band transmission power, or by allowing out-band communications (e.g. in ISM bands).

As for some of the discussed technologies, 4G latest releases include support for D2D communications. 5G, hopefully, will natively support D2D counting on protocols and procedures well optimized (and not as a result of an adjustment) for this technology.
When thinking about D2D paradigm, some unresolved issues rises asking for answer. Starting from the terminals association procedure, if there is BS coverage, then the network can supervise and speed-up discovery and pairing procedures and, at the same time, optimize resource allocation; but to support D2D in non-covered area, devices has to be able to arrange connections in complete autonomy.
In 4G network, downlink and uplink signalling are different, if 5G will follow the same trend, it means that devices will need to be equipped with transmitter and receiver of both downlink and uplink technologies to support D2D, doubling the costs for the transceiver. Moreover, human-centric devices have often different needs for downlink speed and uplink speed; in D2D scenario, where nodes are both provider and consumer of connectivity downlink and uplink performances should instead be symmetric to optimize spectrum usage.

1.2 5G operating modes

As previously mentioned, other than new disruptive technologies which enables very high data-rate communications, 5G means a change in the way mobile networks provide their services.
Since the first mobile cellular generation, mobile networks have always provided, phone-calls and text message services in best effort mode. Everyone has experienced, at least once, the inability to phone or to send or receive messages due to BS congestion in very crowded situations (like sport or music events), or to core network congestion (best example is first minutes of New Year's Day, trying to send SMSs for wishes). As the mobile network started to provide internet connectivity, the situations where the attempts to use internet-based applications fail, happen daily (poor coverage in rural areas, or peak hours in metropolitan areas).

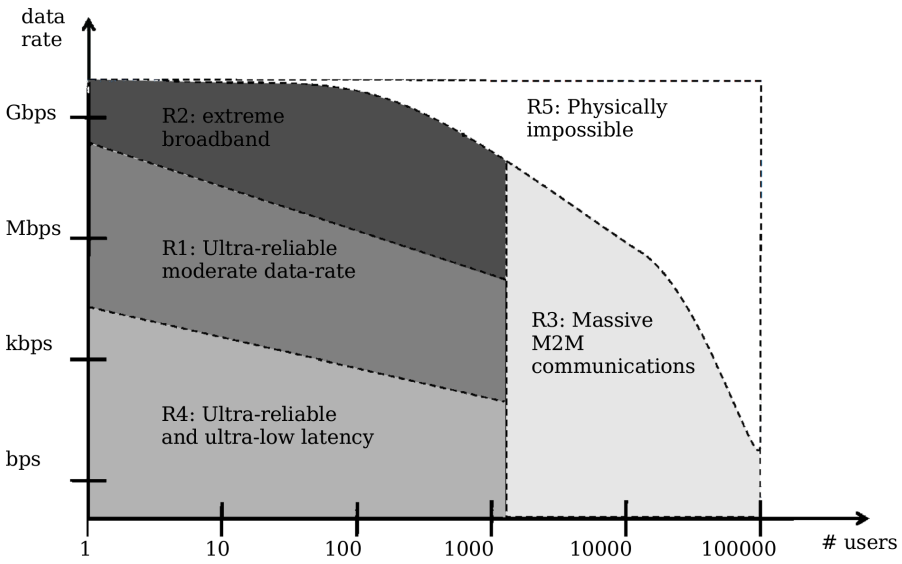

Figure 1.6. *5G operating regions as functions of users and data-rate, values are approximate and only depict the region locations, [26].*

5G will change this paradigm by defining different operating regions, providing different quality of service depending on the end-user needs. Beyond the classical operating mode where wide broadband connections at the best effort is provided, 5G will support a series of so-called Ultra-Reliable-Communications (URC) operating modes.

In Fig. 1.6 the expected configuration for the 5G operating regions is shown. Region 5 represents unachievable operating mode due to physical and information-theoretic limits. Region 1 is the equivalent of the current mobile network operating mode, the data-rate decreases as the population increases, in 5G this kind of operating mode will have some guarantees on the availability of the connection. Region 2 outlines the current pursuit for faster connectivity at the cost of having no guarantee on its availability in special condition (such as crowded environment). Region 3 and 4 describes the M2M requests of either massive devices access or ultra low latency connections.

The ultra-reliable connectivity is a new way of providing internet connectivity: the terminal and the network make an agreement in which the device put some limitations on its behaviour, like low mobility, small message dimensions or tolerant to delay, and the network guarantees a certain level of service. For example in region

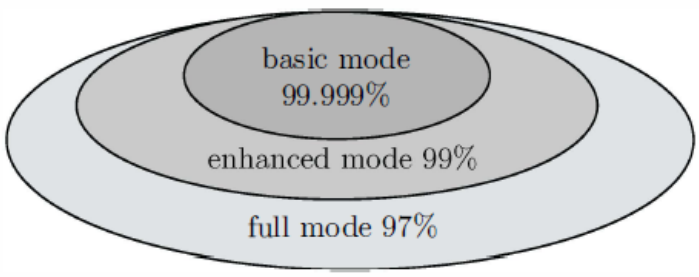

Figure 1.7. *Examples of 5G reliable service composition, [26].*

1, if transmissions are sporadic, minimum data-rate speed will be provided at least 99% of the time, while for example in region 4, if messages are short, they will be delivered within a small latency at least 99.9% of the times.

From an high-level perspective, reliability can be explained as the guarantee that the probability that a certain amount of data will be transferred from one peer to another within a given deadline or time frame will be higher than a certain threshold [26]. Reliability concept leads to the definition of the Reliable Service Composition (RSC), a method to specify different levels of reliable services in order to allow the network to have more degrees of freedoms and the end-user' quality-of-experience to gracefully degrades in case of network problems or momentary congestions.
Fig. 1.7 explains this concept by defining different functionality sets with different percentage of availability. In case, for example, of vehicular communications where the most important constraint is latency, full functionality could represent the case of short messages delivered within short latency, while enhanced functionality could represent longer message with looser time constraints but more restricted constraints on security, and finally base functionality will be all the generic IP-base traffic delivered with minimum data-rate speed.

The URC and RSC paradigms with their promises on transforming mobile connectivity as a truly commodity, available (almost) any time and anywhere, could lead to a total new process of designing protocols for wireless communications. Traditionally wireless protocols, i.e.waveform, signalling, frame structure, etc... are designed with the capabilities to handle all the possible messages and message dimensions; by defining different operating modes, with different sets of limitations and guarantees, wireless protocols can now be designed and tailored to specific mes-

sage types in order to optimize the delivery. Also by having the reliability that some minimum quality of service will be (almost) always available anywhere and any time, mobile applications could be designed in different way and new applications could be built, such as the tactile internet [3].

1.3 Structure of the thesis

Machine Type Communications will play a primary role in driving the design and standardization process of 5G. In this thesis we discuss about two important topics in the field of MTC.
In chapter 2 we discuss on one of the most important application in the field of "critical M2M": wireless vehicular networks. Here the particular purpose of traffic safety and accident prevention impose stringent prerequisites to 5G network on the reliability, availability and latency on the connections among vehicles. As explained in 1.1.7, 5G standard will likely support direct device-to-device communication, including also mechanisms to enable devices to autonomously establish direct connections in case the infrastructure network is not available or misses. These requirements meet the vehicular network scenario where device-to-device communications is a valuable option both in congested situations to offload the base-station, and in rural scenarios where mobile network coverage is poor and being able to establish temporary ad-hoc networks is the only chance to maintain safety of the transportation system.
The analysis aims at showing pros and cons of the vehicular environment. While the extremely dynamic environment of vehicular networks negatively affects the performances of schemes and protocols designed for wireless private networks or mobile networks, this scenario offers opportunities to further optimize the network behaviour by exploiting extra information gathered by electronic systems every modern vehicle is equipped with.
In chapter 3 we consider the field of massive M2M communications where low-energy resource-constrained devices have to last for years on batteries. As a matter of fact many proposals advance the hypothesis to exploit the capillarity of these networks and reduce the amount of energy spent for direct mobile-network connectivity by providing connectivity through alternative protocols such as Bluetooth

or IEEE 802.15.4. In this dissertation we present a protocol stack for M2M devices equipped with more than one radio access technology as the proposals assume. The protocol stack provides IETF-IPv6 features and also includes the 6LoWPAN functionalities for compressing the IPv6 header.
In chapter 4 another aspect of low-energy M2M devices in analysed. Focusing on the energy-saving issue, we study the performances of the hybrid ARQ protocols in terms of outage probability and transmission power allocation in the subsequent transmission attempts. In modern protocols for wireless communications HARQ protocols are widely adopted to increase the final throughput of the communication, they jointly exploit FEC code and ARQ mechanism for retransmission to decrease the final probability of not delivering data correctly.
Using the novel theory on channel coding in finite block-length regime we find the best power allocation strategy for the HARQ protocols and show the advantages, in terms of saved energy, of the such protocols respect to the simple ARQ techniques.

Chapter 2

5G networks and vehicular ad-hoc networks

Inter-vehicular wireless communications will be the principal enabling technology for the future Intelligent Transportation Systems (ITS). Different applications will emerge thanks to the connectivity cars will make available. The main ones will concern the enhancement of road safety and traffic efficiency. By being always interconnected, vehicles will continuously share data about their position speed and direction, thus allowing vehicles to predict and react to possible hazardous situations. For example one vehicle will be able to warn preceding vehicles about dangerous situations, like imminent traffic jam or bad road conditions, granting following vehicles enough time to react properly and safely.

Information about traffic will also be exploited to optimize traffic flows, with the natural consequence of reducing the impact of transportation system on the environment.

This technology will also enable a plethora of new applications, grouped under the name of infotainment applications, that are expected to revolutionize the quality of travelling experience for driver and passengers.

Since 1999, when the FCC reserved 75 MHz bandwidth of wireless spectrum, in the range of 5.9 GHz, for “intelligent transportation applications”, vehicle-to-vehicle (V2V) communications have been under study by the wireless communications community.

As of today the most qualified standard protocols for V2V are all based on the IEEE

802.11p [27] wireless protocol, which is a modified version of the IEEE 802.11a protocol for wireless LAN, and describes the physical and lower-MAC layers for vehicular ad-hoc networks (VANETs).
Many studies have shown limitations of this protocol for vehicular communications, the biggest shortcoming lies in the channel access procedure which is based on the CSMA-CA technique. In [28] and [29] it has been shown that in very crowded situations, the collision probability is too high and the overhead introduced by the back-off time periods enormously increases the inefficiency of the channel access protocol, with the consequence of a drop of the average network throughput.
On the other hand, it has been shown that moving the entire vehicular network traffic to the mobile cellular network could easily congest the serving base station [30].
The only possible solution is an hybrid protocol that supports communications via mobile cellular network and is also able to directly communicate with other peers via device to device protocols.
The mobile cellular network offers the opportunity to apply a centralized management to efficiently allocate resources, particularly effective in metropolitan areas where vehicles density is higher. The D2D communications become useful to offload the mobile network by redirecting the ordinary vehicular network traffic only to nearby vehicles. More important, as long as the D2D protocols include techniques for establishing communications without the supervision of the mobile network, its main contribution is in increasing the network coverage in places where mobile networks are unavailable, allowing the ITS to guarantee safety of vehicles also in rural or remote areas where cellular network coverage is often weak.
As already mentioned, 5G network will be the key technology to enable IoT applications such as inter-vehicular communications. 5G networks will be the springboard for the widespread diffusion of inter-vehicular communications.

In this chapter we present two contributions on vehicular ad-hoc networks, related to aspects of the physical and MAC layers described in the IEEE 802.11p standard protocol.
In section 2.2 we propose a novel channel impulse response estimator that benefits of information retrieved by in-vehicle sensors such as vehicle speed. Thanks to these valuable information we try and estimate the Doppler frequency of the channel im-

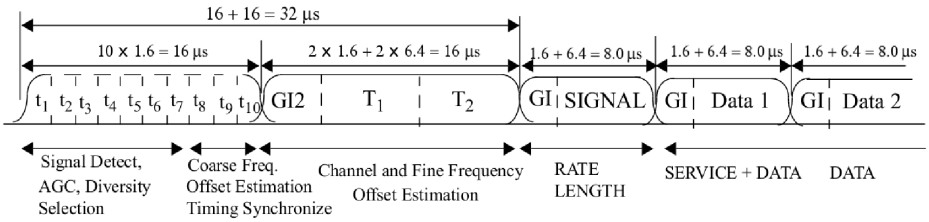

Figure 2.1. *IEEE 802.11p frame structure*

pulse response (CIR) and adapt the CIR estimator accordingly.
In section 2.3 we consider the multi-channel scenario of the vehicular ad-hoc networks. The licensed 75 MHz bandwidth are divided in seven 10 MHz channels which can be accessed simultaneously. We thus analyse different channel occupancy detectors with the aim of finding the best for assessing channels occupancy while preserving the latency requirements of safety messages.

2.1 Vehicular ad-hoc networks

2.1.1 The IEEE 802.11p protocol

The IEEE 802.11p physical layer is based on OFDM and uses $N = 64$ sub-carriers with a cyclic prefix of $N_{CP} = 16$. Different symbol modulation and FEC code puncturing schemes allow transmissions to occur at different rates ranging from 3 to 27 Mbit/s.
To mitigate the Doppler effects due to the vehicular fast-moving environment, the IEEE 802.11p protocol halves the bandwidth from the 20 MHz of the IEEE 802.11a protocol to $B = 10$ MHz, thus the sampling period becomes $T_s = \frac{1}{B} = 100ns$ and the OFDM symbol time period is $T = (N + N_{CP})T_s = 8\mu s$.
Transmissions are frame-based and the frame structure is presented in Fig. 2.1 and Fig. 2.2: every frame starts with a sequence of fixed symbols; the ten-fold repetition of the short sequence $\mathbf{t}_i$, $i = 1, ..., 10$, $\mathbf{t}_i \triangleq \mathbf{t}_s$ is used by the receiver to detect the frame, while the long sequence symbols $\mathbf{T}_1 = \mathbf{T}_2 \triangleq \mathbf{T}_L$ are used by the receiver to perform CIR estimation.
The header symbol denoted in Fig. 2.1 and Fig. 2.2 with the name SIGNAL contains information on the frame length, modulation and coding schemes used in the sub-

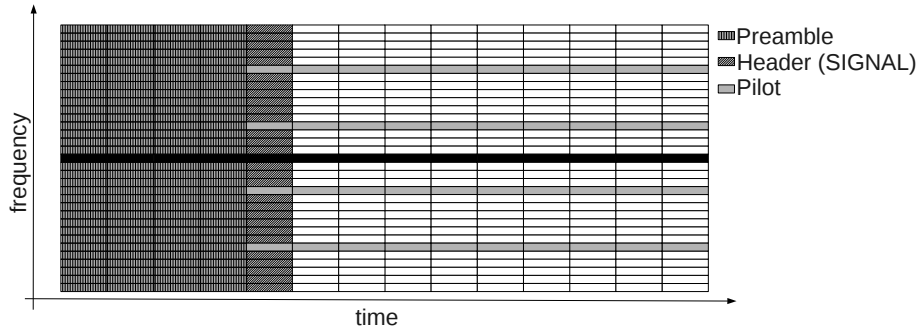

Figure 2.2. *IEEE 802.11p frame structure in frequency and time domain*

sequent payload symbols; it is encoded with the most robust code and modulated using BPSK constellation. The receiver must decode and parse these information before starting to decode the first payload symbol.

2.1.2 Vehicular channel model

Several papers have shown the numerous differences that exist between vehicular wireless channels and the well studied mobile cellular networks channels. Faster channel fluctuations due to both transmit and receive antennae movements, different carrier frequency and different antenna positioning are among the major differences.
Many efforts have been made to characterize the vehicular channel in different scenarios and many models have been presented. In [31] the authors describe how to build a geometric and stochastic mixture model valid only for vehicle to vehicle (VTV) communications in highways scenario.

Here we use the most popular channel model [32], obtained as a result of a very first intensive vehicular channel sounding campaign conducted in different cities within different scenarios, involving highway, urban and rural environments. The model is presented for single antenna systems; it is based on the tapped delay line (TDL) with the WSSUS (wide-sense stationary uncorrelated scattering) assumption, and the Doppler parameters are inferred from vehicles speed. Acosta et al. provide six TDL parameters sets for reproducing the channel impulse responses in different

environments. Channel models have been designed by matching, as much as possible, measured data and TDL statistical parameters like Gaussian processes power, Doppler spectra and shifts. As remarked above, the carrier shift due to Doppler effect can reach, especially in the highway scenario, values above 1 kHz. For this model we use the implementation provided in [33] built upon the IT++ framework [34] where vehicles speed, a tunable parameter, affects the resulting Doppler effects accordingly. Hence, even if not explicitly indicated in [32], we simulated channel impulse responses for different vehicles speed, by properly modifying Doppler parameters of the models.

2.2 Vehicular channel impulse response estimation

As well known, for the performances of any OFDM receiver the channel estimation is critical. However, since the IEEE 802.11p standard inherits most of its features from the well known IEEE 802.11a standard for wireless local area networks, it does not provide sufficient information (e.g. pilot tones) for the purpose of channel tracking. In IEEE 802.11a, wireless links are typically created between an Access Point, always considered in a static position, and terminals, which are assumed having very slow speed - at most 15 km/h - and nomadic behaviors - i.e., stationary for the most of the time. In VANETs terminals are seldom stationary, and they can have a very wide range of speed, from few km/h in metropolitan areas up to 150 km/h in highways. As showed in many papers [35] [36], receiver schemes used for WLANs poorly fits VANETs: higher speed of terminals leads to shorter coherence time of the channel so the initial channel impulse response estimate is valid for a much shorter period.

Furthermore the outdoor scenario of VANETs is in contrast with the typical indoor environment for which the wireless local area networks have been designed: as already pointed out, the coherence bandwidth of the channel is smaller and the pilot tones are too few and too far (in the frequency domain) each other to enable an adequate channel estimation and tracking.

But as we focus our receiver design for VANET-specific devices we can get many advantages: as suggested in the standard, the VANET devices will likely be equipped

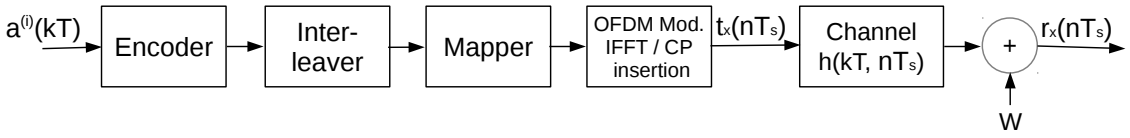

Figure 2.3. *IEEE 802.11p reference system model*

with a GPS sensor to acquire universal time reference; moreover, for safety purposes, they should have direct links with in-car sensors and electronic control units. We first cope with the problem of pilot tones deficiencies by using a parametric channel model and the Least Square Error estimator in the CR estimation process. We then aim to improve the channel tracking process by exploiting information from the in-car sensors and improve the efficiency of the OFDM receiver, in particular we try and estimate the Doppler effect from the information on vehicle speed provided by GPS or speedometer sensors. We focused on Road to Vehicle (RTV) in highway scenario where vehicle speed and Doppler effect have a more direct relationship and we show that considerable improvements in terms of receiver efficiency can be obtained.

2.2.1 System Model

As presented in Fig. 2.3, in our model the received signal is obtained by filtering the transmitted signal $t_x(nT_s)$ with the time-varying channel impulse response (CIR) $h(kT, nT_s)$ and adding white Gaussian noise (WGN) with statistical power such that the signal to noise ratio (SNR) equals:

$$SNR = \frac{P_{tx}}{\sigma_w^2}$$

We focus in the case where perfect time and frequency synchronization between transmitter and receiver is already achieved, we also assume the time-varying CIR to last no more than the CP time:

$$nT_s \geq N_{CP}T_s \implies h(kT, nT_s) = 0, \forall k > 0 \tag{2.1}$$

In this case, neglecting changes in the $h(kT, nT_s)$ during the symbol reception, the OFDM demodulated signal can be expressed in the frequency domain as

$$\mathbf{Y}(k) = \mathbf{H}(k) \cdot \mathbf{X}(k) + \mathbf{W}(k) \tag{2.2}$$

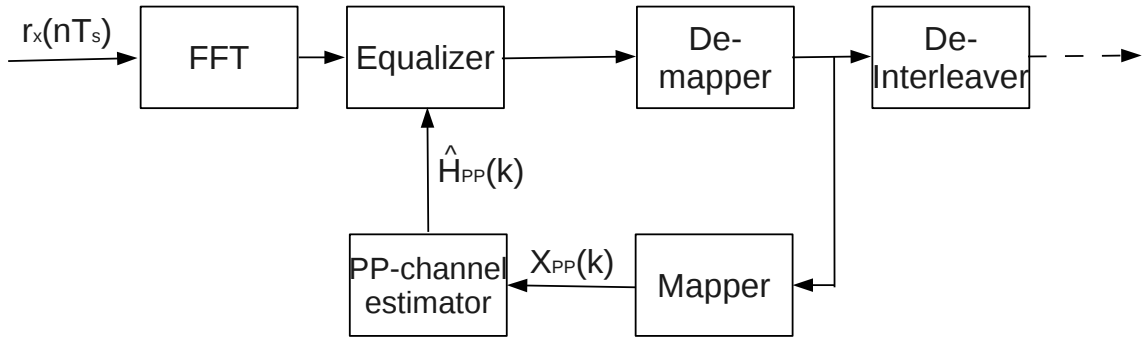

Figure 2.4. *Pseudo-pilot channel estimation block scheme*

where $\mathbf{H}(k)$ is the discrete Fourier Transform (DFT) of the N-element vector $\mathbf{h}(k)$ which is the sampled CIR $h(t, nT_s)\, n = 1, ..., N$ at the time instant kT ; $\mathbf{X}(k)$ is an $N \times N$ diagonal matrix with data symbols $a^{(i)}(k)$ in its diagonal and $\mathbf{W}(k)$ is the additive noise vector.
The most common CRE algorithm is based on Least Square Estimation (LSE): the long training sequence symbols $\mathbf{T}_1$, $\mathbf{T}_2$ can be expressed as:

$$\mathbf{Y}_{\mathbf{T}_1} = \mathbf{H}(0) \cdot \mathbf{X}_{\mathbf{T}_1} \quad \mathbf{Y}_{\mathbf{T}_2} = \mathbf{H}(2) \cdot \mathbf{X}_{\mathbf{T}_2} \tag{2.3}$$

and, applying the Zero-forcing criterion [37, p. 776] the CIR is estimated as:

$$\hat{\mathbf{H}}(0) = \frac{1}{2} \left(\mathbf{Y}_{\mathbf{T}_1} + \mathbf{Y}_{\mathbf{T}_2} \right) \cdot \mathbf{X}_{\mathbf{T}_L}^{-1} \tag{2.4}$$

In WLANs, receivers use $\hat{\mathbf{H}}(0)$ to equalize the whole frame, since the CR can be assumed to be constant for the entire frame reception time.
In Fig. 2.2 the entire IEEE 802.11p frame structure is shown. Within the payload symbols, $L_{pp} = 4$ sub-carriers are filled with a predefined sequence of pilot symbols $p_i(k) \quad i = 1, .., L_{pp}$. The purpose of these symbols is to track drifts in the receiver internal oscillator.

2.2.2 Related works

Many channel tracking mechanisms have been proposed; most of them cope the problem of channel estimation and tracking by proposing new transmission schemes.

In [38], authors suggest to modify the standard and add a mid-amble OFDM symbol every M payload symbols (where M is fixed and depends on the modulation scheme), so the receiver can recompute the CRE periodically. Although it seems the most reasonable solution to the channel tracking problem, it introduces a strong modification to the standard which implies backward compatibility issues.
In [39] authors show the benefits given by a different approach to classical OFDM scheme, using the Differential OFDM (DOFDM) transmission where the demodulation process does not need equalization any more. Assuming the channel impulse response to have small variations between subsequent OFDM symbols, data symbols are demodulated by taking the difference with the previous one in the same sub-carrier. Although this approach shows good performances, the authors does not explain how the transition between the BPSK-modulated header symbol (named as "SIGNAL" in Fig.2.3) and the subsequent symbols, which can be modulated by different constellations, should be handled.
In [40] the authors propose a new algorithm based on the Discrete Prolate Spheroidal (DPS) sequences. Knowing the channel characteristics, the domain of the CR can be tightened to a smaller subset, leading to the definition of a new transfer function whose model can be thought as a convolutional code, iteratively decoded by a BCJR decoder [41]. Although this algorithm theoretically works whatever frame structure, authors show that the current IEEE 802.11p preamble and pilot tones structures are not sufficient to let the decoder converge within a feasible time: the pilot tones distribution does not satisfy the sampling theorem condition, and thus the BCJR decoder must carry out a lot of iterations to reach satisfactory performances, forcing the system to very high computational efforts. Authors conclude by suggesting a backward compatible modification to the standard, which consists in adding a post-amble symbol to the IEEE 802.11p frame, to be used to increase initial information for the decoding algorithm. Even if this solution can be seen as a backward compatible improvement of the standard, adding a post-amble symbol increases transmission inefficiency.
Proposals which does not require modifications to the standard, came up with the common idea to use data-aided pilot tones to solve the problem of the lack of pilot tones, the so-called pseudo-pilot tones (PP tones) construction. As in Fig. 2.4, after the demodulator the OFDM symbols of the frame payload are brought back to the

original values of the constellation and used to fill the $\mathbf{X}_{PP}(k)$ matrix and assess the newer CR estimate with LS estimator:

$$\hat{\mathbf{H}}_{PP}(k) = \mathbf{Y}(k) \cdot \mathbf{X}_{PP}^{-1}(k) \tag{2.5}$$

In [42] the authors propose the "channel smoothing" technique: exploiting (2.1) they use the truncated discrete Fourier Transform DFT (DFT_{TR}) matrix to shrink the last coefficients of the $\mathbf{h}(k)$ vector. $\hat{\mathbf{H}}(k)$ is computed as a double Fourier Transformation of the vector $\hat{\mathbf{H}}_{PP}(k)$:

$$\hat{\mathbf{H}}(k) = DFT\left[IDFT_{TR}\left(\hat{\mathbf{H}}_{PP}(k)\right)\right]$$

where $IDFT_{TR}$ is the truncated inverse DFT.
In [43] the correlation of the evolving CR is exploited to mitigate errors coming from the PP-tones algorithm and the hard symbol demodulation process. With an algorithm similar to the recursive least square filter, authors update the CR by averaging the old estimation with the newer one. To cope with the noise in low SNR conditions an extra cycle of frequency-domain averaging is made before the time-domain averaging step. They average the per-sub-channel coefficients of the estimated CR with the adjacent ones:

$$\hat{\mathbf{H}}_{up}^{(i)}(k) = \frac{1}{2\beta+1} \sum_{t=i-\beta}^{i+\beta} \hat{\mathbf{H}}_{PP}^{(t)}(k)$$

and then make the final step: the recursive average in the time domain

$$\hat{\mathbf{H}}_{STA}(k) = (1-\gamma)\,\hat{\mathbf{H}}_{STA}(k-1) + \gamma\hat{\mathbf{H}}_{up}(k)\ .$$

Since the averaging is made both in frequency and time domain, they call the method "Spectral temporal averaging" (STA).
In [44] the authors present "Constructed data pilot" (CDP) method, where an heuristic algorithm exploits the time correlation of the channel. The first CRE $\hat{\mathbf{H}}_{CDP}(0)$ is obtained by (2.4).
The sub-sequent CREs are computed by comparing the equalization results on the same received OFDM symbol $\mathbf{Y}(k)$ of the vectors $\hat{\mathbf{H}}_{CDP}(k-1)$ and the vector $\hat{\mathbf{H}}_{PP}(k)$ (2.5); if the demodulator decides for the same symbol in both cases then

$$\hat{\mathbf{H}}_{CDP}^{(i)}(k) = \hat{\mathbf{H}}_{PP}^{(i)}(k)$$

otherwise

$$\hat{\mathbf{H}}^{(i)}_{CDP}(k) = \hat{\mathbf{H}}^{(i)}_{CDP}(k-1)$$

The previously mentioned data-aided estimation algorithms are based on the demodulator performance which is heavily influenced by the SNR level of the received signal. The catastrophic effects due to errors in symbol demodulation bring the channel estimators to compute the matrix $\mathbf{X}(k)$ from wrong symbols, generating a wrong CRE, which, as a consequence, brings the symbol demodulator to make much many errors in the next iteration.
We also noticed the complete absence of any consideration about the coherence time of the CR. In the STA algorithm the parameter γ is constant and independent from the vehicle speed, and the recursive estimation of the CRs intrinsically considers the channel to be time correlated even for infinite time lapses. In the CDP algorithm there is no theoretical analysis about the coherence time, and the time correlation is only implicitly exploited during the comparison of the equalization results.

2.2.3 proposed scheme

A first improvement to the aforementioned methods is to include the decoding and re–coding steps in the cycle of pseudo-pilot channel estimation.
As well known the decoder introduces a delay which is at least equal to the constraint length L_{CC} of the transmitter encoder, so for every incoming OFDM symbol we only have at most the first $D = N - L_{CC}$ symbols; the computation of the CR as in (2.5) becomes then impossible, since the matrix $\mathbf{X}(k)$ is only partially available, with uncertainties on the number and placements of the missing values.
As showed in [45] channel reconstruction techniques like spline or linear interpolation are error prone in case of wide spaced or not equally spaced pilot tones.
Thanks to sparse vector estimation and the algorithm described in [46], we can overcome this problem.
The expression (2.2) can be rewritten (omitting the additive noise) as:

$$\mathbf{Y}(k) = \mathbf{X}(k) \cdot \mathbf{W} \cdot \mathbf{h}(k) \tag{2.6}$$

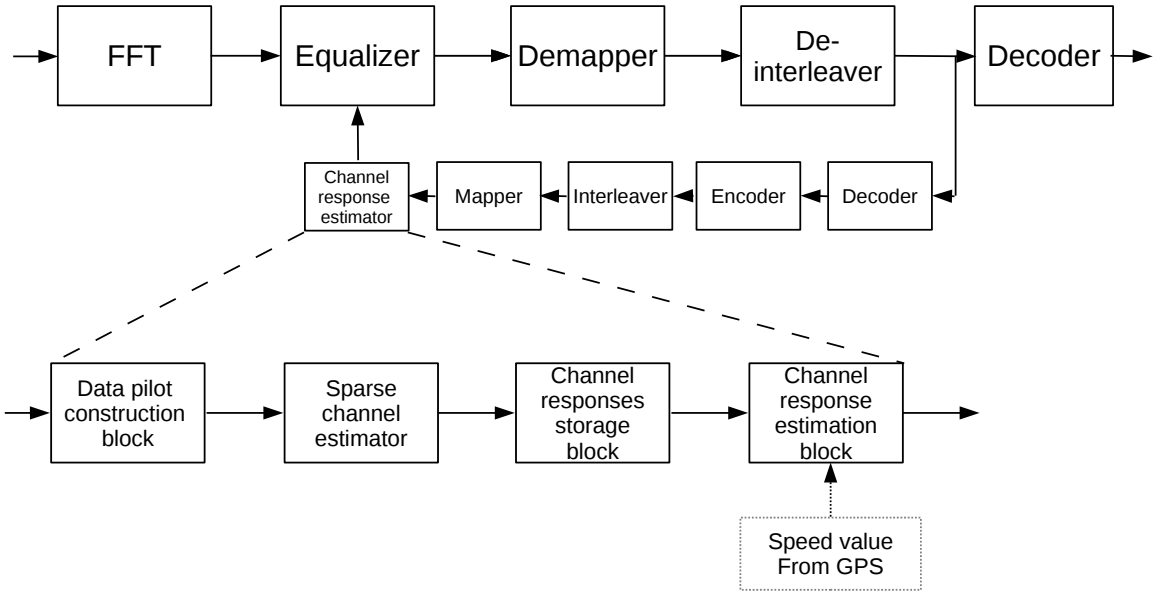

Figure 2.5. *Structure of the proposed receiver*

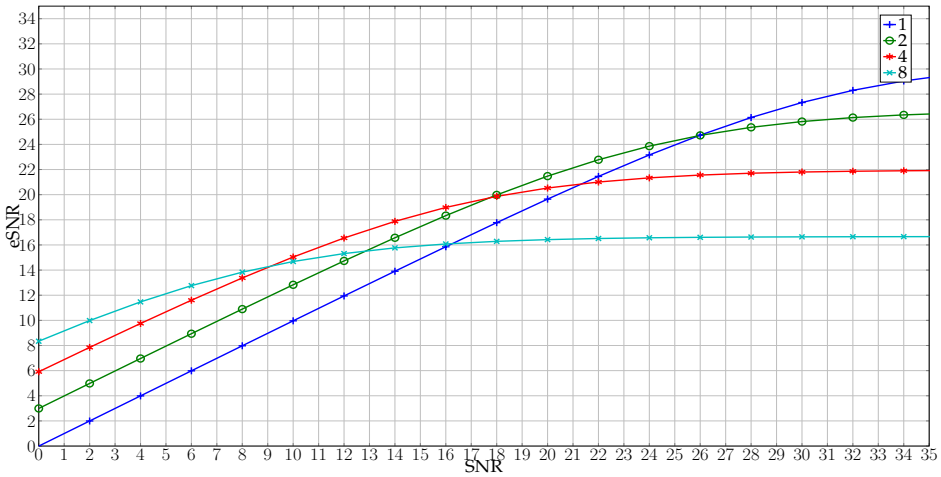

Figure 2.6. *$eSNR$ with respect to real SNR at a vehicle speed of 100 km/h for different channel update rates*

where vector $\mathbf{h}(k)$ has length L_{ch} and $\mathbf{W}$ is the $N \times L_{ch}$ truncated DFT matrix. In fact, we fairly suppose the impulse response to have only the first L_{ch} coefficients to be non null as confirmed in [32] [47] [48] where the authors state that the vehicular CIR typically never last more than 1000 ns, (i.e. exactly 10 samples at 10 MHz sampling rate). So we remove the null coefficients from the $\mathbf{h}(k)$ vector and the last $N - L_{ch}$ columns from the $\mathbf{W}$ DFT matrix.
We must also take into account the fact that the $\mathbf{X}(k)$ matrix contains only $D < N$ valid data, so we build the selection matrix $\mathbf{S}$ with dimension $D \times N$, which extracts the non null elements of the $\mathbf{X}(k)$ matrix. We rewrite (2.6) as:

$$\bar{\mathbf{Y}} = \bar{\mathbf{X}} \cdot \bar{\mathbf{W}} \cdot \mathbf{h}$$

where

$$\bar{\mathbf{Y}} = \mathbf{S} \cdot \mathbf{Y}, \qquad \bar{\mathbf{X}} = \mathbf{S} \cdot \mathbf{X} \cdot \mathbf{S}^T, \qquad \bar{\mathbf{W}} = \mathbf{S} \cdot \mathbf{W}$$

If $D \geq L_{ch}$, for every incoming OFDM symbol k, we can retrieve $\mathbf{h}(k)$ using the normal equation:

$$\hat{\mathbf{h}}(k) = \left[\left(\bar{\mathbf{X}}(k) \cdot \bar{\mathbf{W}} \right)^H \cdot \bar{\mathbf{X}}(k) \cdot \bar{\mathbf{W}} \right]^{-1} \cdot \left(\bar{\mathbf{X}}(k) \cdot \bar{\mathbf{W}} \right)^H \cdot \bar{\mathbf{Y}}(k) \tag{2.7}$$

And finally we obtain the CR estimation in the frequency domain as:

$$\hat{\mathbf{H}}(k) = \mathbf{W} \cdot \hat{\mathbf{h}}(k) \tag{2.8}$$

We called this modified version of the algorithm presented in [46], PP-MMSE to underline the fact that channel estimation is based on data-aided pilot tones also known as pseudo-pilot (PP) tones.
The condition:

$$D \geq L_{ch} \tag{2.9}$$

is a necessary condition, if not fulfilled the matrix

$$\mathbf{Z}(k) = \left(\bar{\mathbf{X}}(k) \cdot \bar{\mathbf{W}} \right)^H \cdot \bar{\mathbf{X}}(k) \cdot \bar{\mathbf{W}}$$

would not be full rank and it can not be inverted. $\mathbf{Z}(k)$ is also related to the variance of the estimation. The LS estimator theory [49, p. 47] the model parameters:

$$\beta = \left(X^H X \right)^{-1} X^H y$$

have variance equal to:

$$var\left(\beta\right) = \sigma^2 \left(X^H X\right)^{-1}$$

where σ^2 is the noise variance and the matrix $\left(X^H X\right)^{-1}$ can be interpreted as the estimation of the covariance matrix of the input vector x, which, in our case, correspond to the transmitting symbols. We can thus, rewrite the final variance of the estimated parameters β as:

$$var\left(\beta\right) = \frac{\sigma^2}{N cov(x)}$$

and conclude that to reduce the variance and enhance the estimation reliability, we can only act on the number N of the input matrix X. This means in practice, that the more the matrix X in (2.6) is close to be a full rank $N \times N$ matrix, the less will be the estimation error of the CR (2.8).

The choice of the trellis depth (depending on the constrained length of the code) of the Viterbi decoder must guarantee a number of valid symbols per OFDM frame $D \geq L_{CC} - L_{pp}$.

For every incoming OFDM symbol the receiver decodes the symbols with the extra Viterbi decoder, pads with zeroes the vector of length D to obtain the right dimension N, then data are re–encoded and re–interleaved. Based on the interleaver shuffling pattern, the pilot construction block selects the sub-carrier indexes which contain valid data. It also builds the DFT sparse matrix $\mathbf{W}$, used by the following block to compute the $\mathbf{\hat{H}}(k)$ response according to (2.7) and (2.8).

As mentioned we also focus the receiver design to the VANET scenario and exploit further information about vehicle status to improve performances; in particular we are interested in the vehicle speed provided by GPS receiver to estimate the Doppler effects' parameters.

A non-zero speed between transmitter and receiver is the principal cause of Doppler effects, which gives rise to frequency shift and frequency broadening of the received signal [50, p. 88]. The Doppler Spectrum describes this phenomena in terms of the probability density function (pdf) of the incident waves' magnitude at the different frequencies within the signal bandwidth. In case of non line-of-sight (NLOS) communication, Rayleigh pdf is used and the relative Doppler spectrum is the well

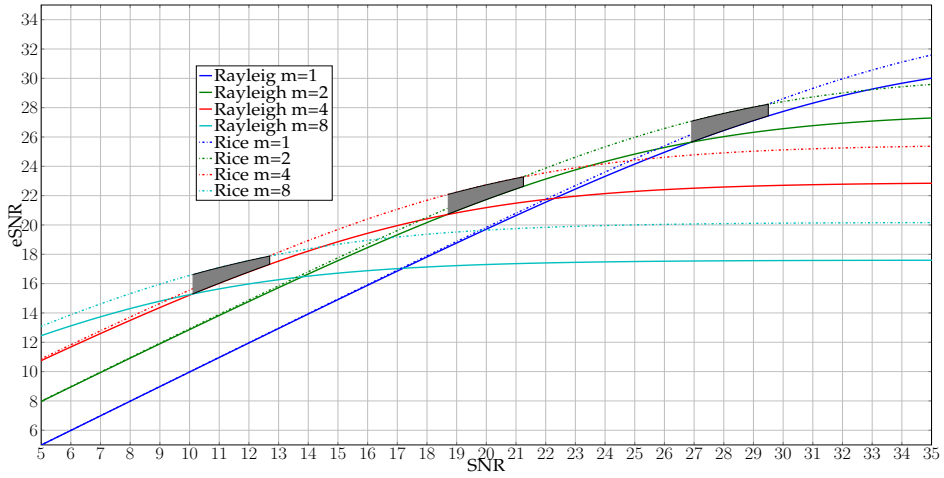

Figure 2.7. *$eSNR$ with respect to real SNR at a vehicle speed of 100 km/h for different channel update rates, Rice compared to Rayleigh processes*

known Jake's Model:

$$D(f) = \begin{cases} \frac{1}{\pi f_D \sqrt{1-(f/f_D)^2}} & |f| \leq f_D \\ 0 & otherwise \end{cases}$$

where f_D is the maximum frequency of the Doppler spread. On the contrary if there exists a dsominant component the Rice process best suits the LOS communication scenario. Here we assume the communication to be in NLOS and we follow the procedure described in [51]; where the authors approximate every tap Doppler spectrum with the Jakes model. Then we will show that for our purposes, the error we are making in not considering a LOS communication is negligible.
From the Jake's spectrum the auto-correlation function of the CIR in the continuous time domain is equal to [37, p. 313]:

$$r(\Delta t; \tau) = \int h(t, \tau) h^*(t + \Delta t, \tau) dt = \tag{2.10}$$

$$\sum_{n=1}^{L_{ch}} = \sigma^2_{\tau_n} J_0(2\pi f_D \Delta t) \delta(\tau - \tau_n)$$

where $\sigma^2_{\tau_n}$ is the energy associated to a given delay τ_n, and $J_0(x)$ is the zero-order Bessel function.
In the discrete time domain the CIR becomes:

$$h_n(t) = h(t, nTs)$$

and the correlation function (2.10) becomes:

$$r_{h_n}(\Delta t) = \sigma_{h_n}^2 J_0(2\pi f_D \Delta t) \tag{2.11}$$

The difference between the tap coefficient at time t and at time $t + \Delta t$ is:

$$\Delta h_n(\Delta t) = h_n(t) - h_n(t + \Delta t)$$

with statistical power equal to:

$$E\left[||\Delta h_n(\Delta t)||^2\right] = 2\sigma_{h_n}^2 \left(r_{h_n}(0) - r_{h_n}(\Delta t)\right)$$

Assuming the channel filter energy equal to 1 we calculate the variance of the error we would make if we do not update the CIR for a certain number of OFDM symbols m:

$$\sigma_h^2(mT) = \sum_{l=0}^{L_{ch}} 2\left(r_{h_n}(0) - r_{h_n}(mT)\right) = 2\left(1 - J_0(2\pi f_D mT)\right) \tag{2.12}$$

Our key idea is to use the current vehicle speed to infer the f_D parameter by using the formula

$$f_D = f_c \frac{v}{c}$$

where f_c is the carrier frequency, c is the speed of light, and v is the vehicle speed acquired from the GPS or in-car sensor. We also suppose that if we do not update the channel for a given number of symbols, we are implicitly considering the CR constant for that time period, thus we can fairly average the estimated CRs to reduce the estimation variance.

We conclude that a time-averaging operation of sub-sequent CR estimations, induces two opposite effects: reduction of the additive noise power, and increase of the estimation variance due to CR changes. For a certain SNR level, we calculate the experienced SNR value $eSNR$ as:

$$eSNR(m) = \frac{1}{\frac{1}{m}\left(\frac{1}{SNR} + \sum_{k=1}^{m} \sigma_h^2(kT)\right)} \tag{2.13}$$

In Fig. 2.6 the $eSNR$ with respect to real SNR is shown; for an update rate of $m = 1$, $eSNR$ is almost equal to real SNR except for high SNR values where the channel variability within the single OFDM symbol is noticeable.

In practice, for every incoming frame our receiver estimates the SNR level from the long training sequence symbols as:

$$SNR = \frac{1}{2N} \sum_{n=1}^{N} \|Y_{T_1}^{(n)} - Y_{T_2}^{(n)}\|^2$$

as explained in [52]; then using (2.13) with different value of m, it seeks for the best channel updating rates, i.e. the updating rate which guarantees the highest value of the $eSNR$.

To analyze the case of a LOS communication we have first to change the per-tap auto-correlation function (2.11).The first coefficient h_1 includes a dominant component due to the LOS path and the Rice distribution should be used, the (2.11) should be substituted with the formula in [53]:

$$r_{h_n}(\Delta t) = \sigma_{h_n}^2 \frac{I_0\left(\sqrt{\kappa^2 - 4\pi^2 f_D^2 \Delta t^2 + j4\pi\kappa f_D \Delta t}\right)}{I_0(\kappa)} \tag{2.14}$$

where κ represents the power ratio between the LOS components and the scatterers, and it is easy to show that with $\kappa = 0$, (2.14) becomes (2.11). Taking the real part of the auto correlation function (2.14), and following the same procedure as for the NLOS case, the final formula for the error variance (2.12) becomes:

$$\sigma_h^2(mT) = 2\left[1 - \left(1 - \sigma_{h_1}^2\right) J_0(2\pi f_D mT)\right] - \sigma_{h_1}^2 \frac{I_0\left(\sqrt{\kappa^2 - 4\pi^2 f_D^2 \Delta t^2 + j4\pi\kappa f_D \Delta t}\right)}{I_0(\kappa)} \tag{2.15}$$

where $\sigma_{h_1}^2$ is the fraction of the energy of the first tap respect to the total channel energy. Finally if we substitute $\sigma_h^2(mT)$ in (2.13) we obtain the experienced $eSNR$ in case of NLOS communications.

Even though, the second-order statistics of Rayleigh and Rice processes are quite different, in our case the error we make by always considering a NLOS communication is still moderate and bounded in particular situations. In fact, we are not interested in the value of $eSNR$ but in the rate m which maximize (2.13); so the error we make is located only where the best update rates for NLOS and LOS communications are different.

In Fig. (2.7) we show the locations of the error for $\kappa = 10$. The grey areas evidence the SNR zones where we encounter errors and give an idea of the loss of SNR we

face by selecting the wrong value of m. Hence, to avoid increasing the complexity due to κ factor estimation ([54][55]), the receiver can always assume a non-LOS communication, and computes the channel update rate through (2.13).

The final receiver structure is shown in Fig. 2.5: from the main receiver chain, demodulated symbols are passed to the extra Viterbi decoder. The output is then padded with zeros to obtain the right length for the interleaver and symbol mapper. The reconstructed OFDM symbol is then processed by the PP-MMSE algorithm which returns $\hat{\mathbf{H}}(k)$, the vector is stored in a circular memory buffer which saves the last m vectors $\hat{\mathbf{H}}(k)$. The last block, exploits the vehicle speed and averages the responses and finally passes the current CR estimation to the equalizer.

2.2.4 Simulation setup

We used the channel model implementation provided by [33]. We limited our simulations to RTV in highway scenario, considering a vehicle speed of 150 km/h. For such a scenario, we simulated transmissions with different modulation techniques, adopting the most robust coding scheme; we build two frames with different payload lengths: the former with 200 OFDM symbols to simulate a typical IPv6 packet transmission for infotainment applications. The latter with 50 OFDM symbols to reproduce the transmission of packets for safety applications.
We compared our solution to the aforementioned receivers; we simulated as well a common WLAN receiver where no tracking technique is used. We set the STA [43] and CDP [44] parameters as suggested by the authors, in order to ensure the best performances. We assume the receivers are synchronised both in time and frequency.
The extra Viterbi decoder trellis depth has been selected to be a multiple of the inverse of all the possible coding rates to avoid problems in the zero padding process due to fractional bits. As mentioned, we have selected the longest depth that guarantees the PP-MMSE algorithm to work in every transmission scheme (2.9), which it turns out to be 18. We set the available channel update rates to include at most 8 symbols since an higher rate does not show relevant improvements, while costing more in terms of memory. We also pruned the set to be $\{1, 2, 4, 8\}$ to simplify averag-

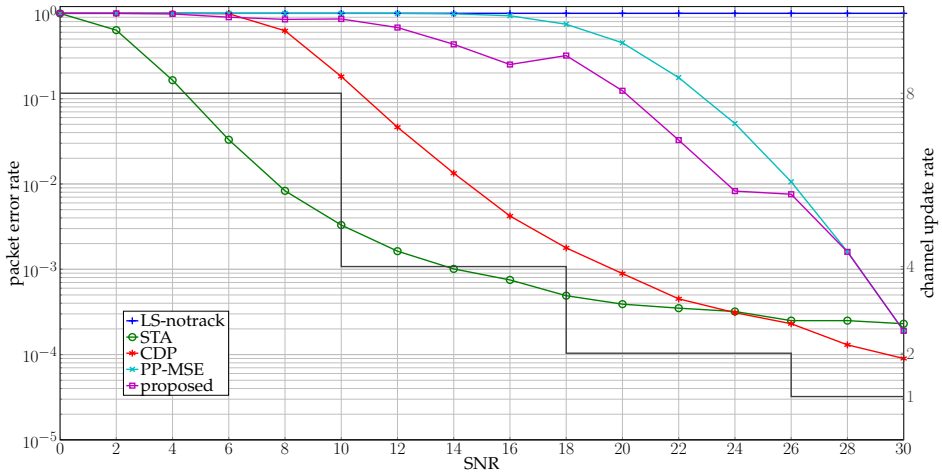

Figure 2.8. *packet error rates for 50 OFDM payload symbols frames; BPSK modulation is used, and the vehicle travels at 150 km/h. The piecewise constant line represents the selected channel update rates based on $eSNR$*

ing operations. To highlight the improvement given by the speed data exploitation, we also simulated the receiver performance without the averaging step, i.e. removing the channel storage block showed in Fig. 2.5.

2.2.5 Results

As a first note, in all the figures (Fig. 2.8, Fig. 2.9, Fig. 2.10, Fig. 2.11, Fig. 2.12 and Fig. 2.13) we can see that the classical WLANs receiver does not work in the VANET environment, no matter the choice of the modulation or SNR level.
In Fig. 2.8 and Fig. 2.9 packet error rates (PER) results with BPSK modulation are shown; in this case the proposed receiver and the PP-MMSE receiver show very poor performances compared to others: this happens because of the channel estimation block. This particular transmission scheme provides only few valid subcarrier indexes - 12 indexes - worsening the performances of the PP-MMSE channel estimator; in this case the only possible solution would be to shorten the depth of the Viterbi decoder; however we think that the reward of improving the results in this scenario are not worth the deterioration we would have in all other modulation schemes.
The up-and-down slope of the proposed scheme in both Fig. 2.8 and Fig. 2.9 hap-

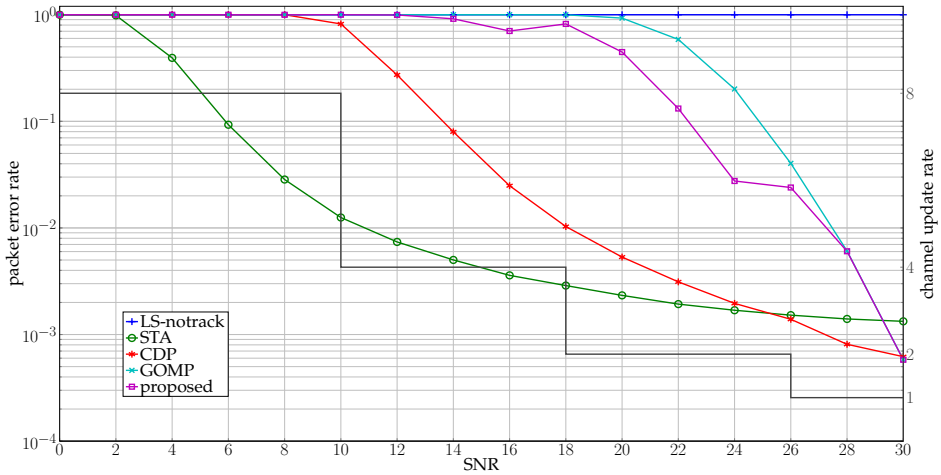

Figure 2.9. *packet error rates for 200 OFDM payload symbols frames; BPSK modulation is used, and the vehicle travels at 150 km/h. The piecewise constant line represents the selected channel update rates based on $eSNR$*

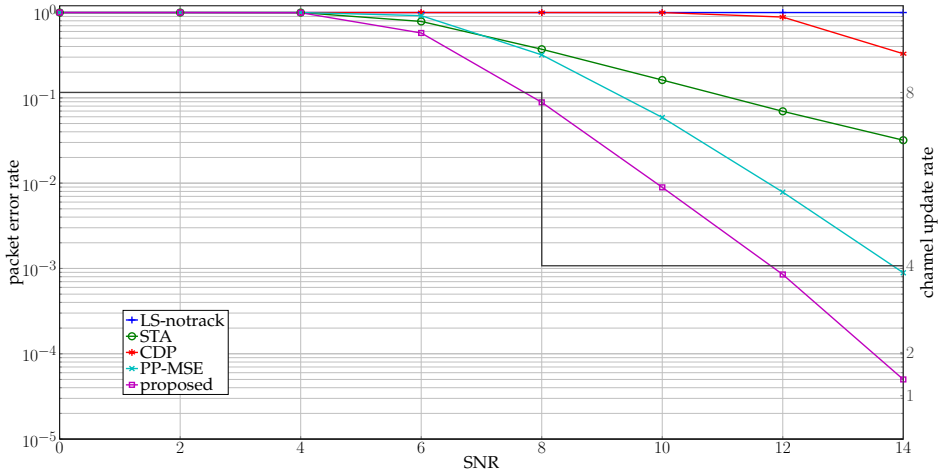

Figure 2.10. *packet error rates for 50 OFDM payload symbols frames; QPSK modulation is used, and the vehicle travels at 150 km/h. The piecewise constant line represents the selected channel update rates based on $eSNR$*

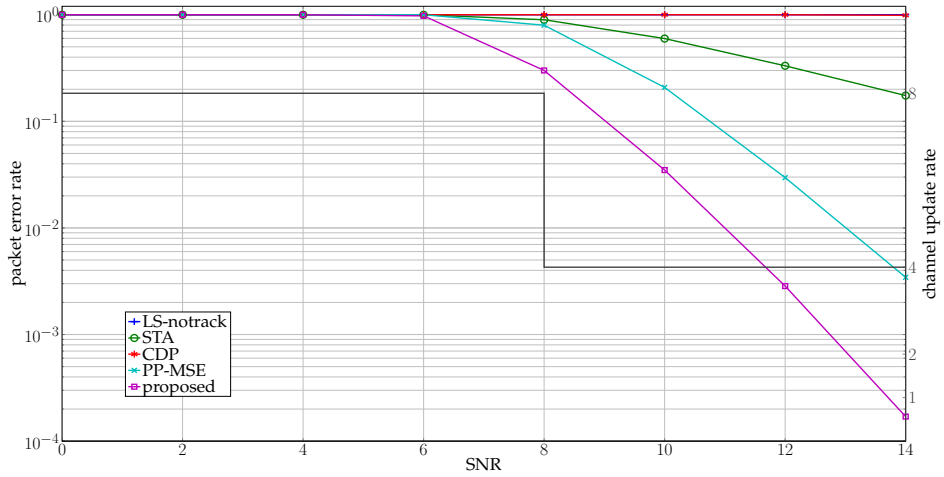

Figure 2.11. *packet error rates for 200 OFDM payload symbols frames; QPSK modulation is used, and the vehicle travels at 150 km/h. The piecewise constant line represents the selected channel update rates based on $eSNR$*

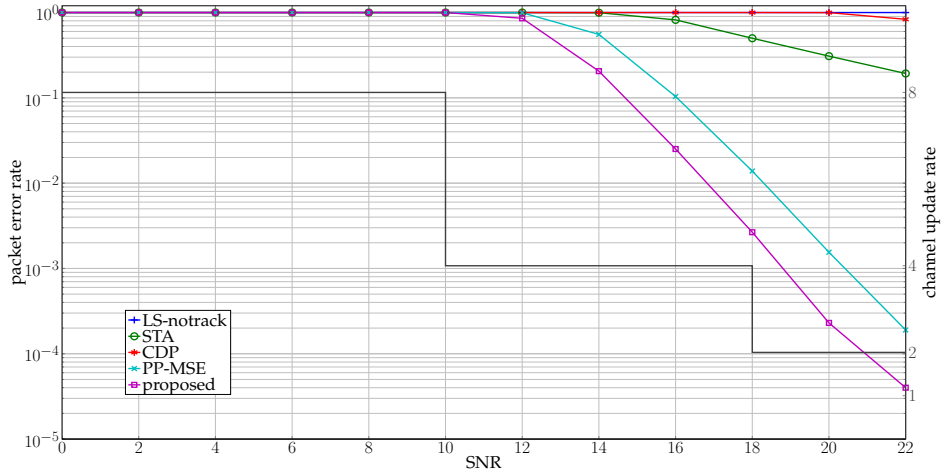

Figure 2.12. *packet error rates for 50 OFDM payload symbols frames; 16-QAM modulation is used, and the vehicle travels at 150 km/h. The piecewise constant line represents the selected channel update rates based on $eSNR$*

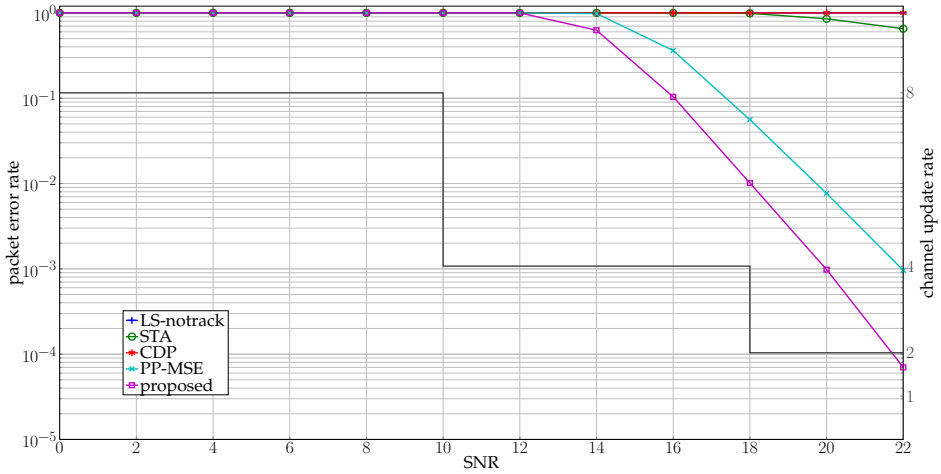

Figure 2.13. *packet error rates for 200 OFDM payload symbols frames; 16-QAM modulation is used, and the vehicle travels at 150 km/h. The piecewise constant line represents the selected channel update rates based on $eSNR$*

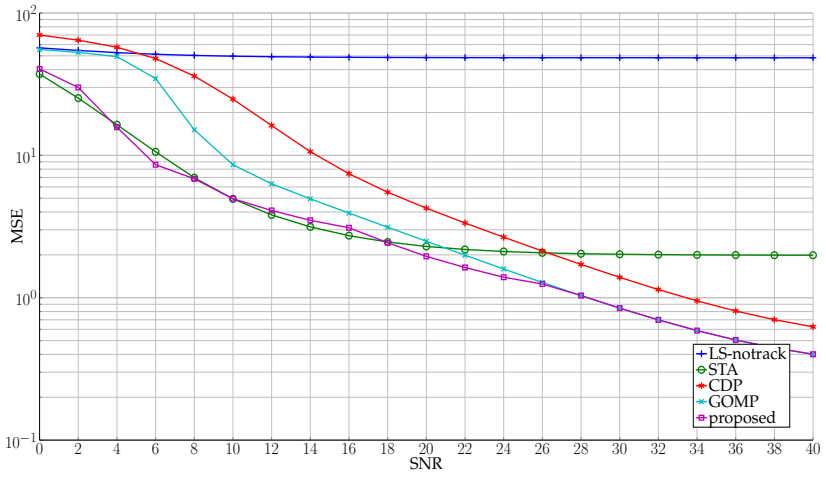

Figure 2.14. *Channel estimation mean squared errors comparison, for the proposed receiver schemes. The transmission scheme used is QPSK with code rate $\frac{1}{2}$ as in Fig. 2.10*

pens exactly at the point where the channel averaging rate changes from the current level to the next one, finally reaching, as expected, the same performances of the PP-MMSE receiver when the rate becomes 1.
In Fig. 2.10 and Fig. 2.11, performances of the reception of QPSK-modulated frames are shown; the proposed receiver achieves the best performances. Here the Viterbi decoder provides 28 valid sub-carriers per OFDM symbol, guaranteeing to the PP-MMSE algorithm enough data to compute a precise channel estimation. The PER shows the improvement due to channel averaging: the gain is about 2 dB.
Comparing Fig. 2.10 and Fig. 2.11 with Fig. 2.8 and Fig. 2.9 it can be noticed that the proposed receiver obtains better results with the QPSK transmission than with the BPSK one. Fig. 2.8 and Fig. 2.9 show that even the STA and CDP receivers in the BPSK scenario have worse performances than the proposed scheme with the QPSK.
In Fig. 2.12 and Fig. 2.13 a 16-QAM transmission has been used; here the number of valid sub-carrier indexes reaches 32, and the gap between proposed receivers and the other ones becomes greater. On the contrary the enhancement due to channel averaging keeps the same: 2 dB as the PER curve starts to decrease.
In Fig. 2.10, Fig. 2.11 Fig. 2.12 and Fig. 2.13, improvements of the PP-MMSE algorithm in data symbols reconstruction are shown. As previously mentioned, hard demodulation shows weakness in low SNR scenarios; by including the decoder in the channel estimation process, data-aided pseudo-pilot tones are less error prone. As a consequence the PER of the PP-MMSE and proposed receivers start their descending slope at lower SNR values respect to the STA and CDP receivers.
In Fig. 2.14 mean squared error ratios of channel estimates are compared. Since all channel estimation algorithms are based on the pseudo-pilot algorithm which assumes that the modulation scheme is known, the error has been computed only on frames for which the frame headers have been decoded correctly and the modulation scheme has been recognized. At low SNR values, the STA receiver performances are comparable with the ones of the proposed receivers, while as the SNR increases, the STA receiver reaches an asymptotic value and the error gets flat. This trend compared with the PER performances seems to conflict, the cause may lays in the averaging process of the channel estimator: even if the channel estimation shows robustness to symbol errors in case of low SNR, it bounds the performances in case of high SNR values where channel variability is predominant.

2.2.6 Final remarks

We showed a novel approach, in which information taken from external sensors are used to improve the receiver efficiency. We focused on a specific scenario, the RTV, where channel variance and Doppler effects are strictly connected to vehicle speed. The RTV scenario pays an important role in vehicular networks, especially regarding to safety. Improving receiver performances in such a scenario means warning drivers more in advance, providing more time to react to dangers. We simulated different transmission rates and demonstrated that the channel update rate must be chosen based on the Doppler spread and not on the modulation technique as previous proposals have done.

2.3 Vehicular ad-Hoc networks in a multichannel scenario

The IEEE 802.11p MAC layer standards have been deeply studied in critical situations, and the common conclusion is that neither the minimum delay nor the maximum throughput or maximum multichannel exploitation is achieved.
In [28], [29] and [56] authors exposed all limits and still open issues of the IEEE 802.11p standard used in VANET. As mentioned previously, the CSMA/CA scheme used in VANET does not fit well the broadcast nature of VANET data, mainly because of the lack of adaptive congestion window and retransmissions mechanisms, since no failed transmission can be detected. From that, we can conclude that the need of a quick and reliable mechanism to sense all the available bandwidth with the aim to draw a map with a congestion index for every channel is a mandatory feature to be added in VANET to enable a reliable and timely delivery of safety messages. This problem essentially can be formulated as the problem of finding the most suitable channel i.e. the channel where less terminals are active. The problem can be re-stated as the problem of detecting the energy in each channel and selecting the one with less energy, assuming that the energy in the channel is a reliable measure of how many terminals are using the channel itself.

From cognitive radio researches, it is well demonstrated that cooperative detection - a possible solution for our problem - has better performances than single sensor detection. In [57] the cooperative detection is proposed even in vehicular networks. Unfortunately, especially in VANETs which are very sensitive to an increase in volume of data to share, benefits from cooperative detection can be overtaken from overhead due to detection information exchange (in particular in an uninfrastructure network). As a consequence, here we consider the five most popular cognitive radio detectors and evaluate their performances in VANETs, simulating both urban or highway scenarios. To help framing the problem in the context of cognitive energy detection, we remark that - according to the standards employed in our application - the sensing can be performed in the 50ms SCH interval where VANET terminals are transmitting in service channels, and the whole bandwidth must be sensed and classified. The problem we are facing then becomes harder and harder since the maximum time interval which we can use to detect the energy level in one channel is reduced as the number of service channels increase.

2.3.1 Cognitive radio detectors

2.3.1.1 Energy detector

The problem of detecting a signal within noise, for which we only know the band in which it is, is firstly considered in [58] where the author proposes an energy detector which does not require any prior knowledge about the transmitted signal; on the contrary, the noise is supposed to be a flat band-limited white Gaussian noise with a known maximum power. The proposed energy detector, which will be referred to as *ES* detector, samples the channel, collecting power levels, for a given time interval: in case of no transmitted signal the statistics of the sum of the samples follows a central chi-squared distribution; if any signal is present, the statistics follows a non-central chi-square distribution. Knowing the noise power level, a threshold for a specific false alarm probability η_{es} can be easily found. Detection is then performed by simply comparing:

$$\frac{1}{N}\sum_{i=1}^{N}|x_i|^2 \lessgtr \eta_{es}$$

where:

- N is the number of collected samples
- x_i is the *i-th* collected sample.

The threshold η_{en} can be computed as:

$$P_{fa} = Q\left(\sqrt{N}\frac{\eta_{es} - \sigma^2_{noise}}{\sigma^2_{noise}}\right)$$

where:

- P_{fa} is the desired probability of false alarm
- Q is the classical Q-function
- σ^2_{noise} is the noise variance

To the author knowledge, this is the simplest detection method, it does not need any further information than the noise power level and number of samples to collect; it does not involve complicated digital operations, so it can be even implemented in analogue domain (the summation becomes an integral); on the contrary it does not exploit any further information about the signal to be detected and in low SNR conditions it may become unreliable.

2.3.1.2 Detection based on second-order statistics

OFDM (Orthogonal Frequency Division Multiplexing) [37] signalling is nowadays the most common modulation used in most wireless communications systems. As a matter of fact IEEE 802.11p, the physical layer for VANET, employs OFDM signalling. It is well known that OFDM employs a cyclic prefix, i.e. the last part of the packet is prepended to the packet itself; the cyclic prefix then has a strong correlation factor with the OFDM symbol, which can be exploited by calculating a coefficient R_i which gives the average correlation factor among the collected samples:

$$R_i = \frac{1}{K}\sum_{k=0}^{K} r_{i+k(N_s+N_{cp})} \qquad r_i \triangleq x_i^* x_{i+N_{cp}}$$

where:

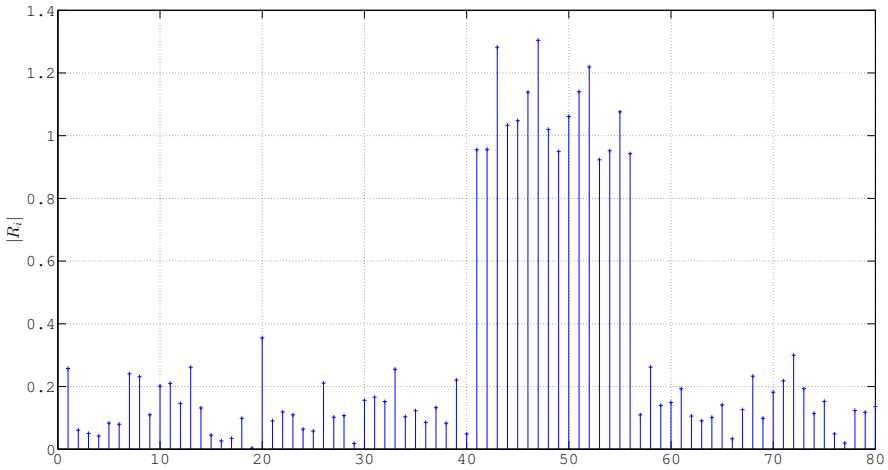

Figure 2.15. *R absolute value computed over 50 contiguous IEEE 802.11p OFDM symbols, τ equal to 40*

- N_s is the length of the OFDM symbol without the cyclic prefix
- N_{cp} is the length of cyclic prefix
- K is the maximum number of complete OFDM symbols within the N collected samples.

The statistics of R_i has been well studied in [59]. Axell *et al.* notice that only for N_{cp} every $N_s + N_{cp}$ samples, R_i values are high, once again as a consequence of the correlation of the cyclic prefix, as explained. The position of the N_{cp} samples depends on the time delay between the first collected sample and the first transmitted sample of the OFDM symbol. Although in the literature, many detectors have been proposed to exploit the R_i statistics, we choose two of them: the auto-correlation detector and the sequential quickest detector. In the following we quickly review them.

2.3.1.3 Auto-correlation detector

In [60] an empirical mean Y of the R_i, normalized by the average signal power, is first calculated:

$$Y \triangleq \frac{\sum_{i=0}^{N_s+N_{cp}-1} \Re\left(R_i\right)}{\frac{N_s+N_{cp}}{N} \sum_{i=0}^{N-1} |x|^2} \lessgtr \eta_{ac}$$

This detector, henceforth called *AC* detector, has the advantage that it does not require an a priori knowledge of the power level. However it does not consider the fact that under the hypothesis of signal presence the observed samples has a non-stationary statistics, a matter which could reduce performances in low SNR conditions.

2.3.1.4 Generalized log-likelihood ratio test

In [59] a generalized log-likelihood ratio test (GLRT) against a threshold η_{GLRT} is proposed; instead of taking the mean as in auto-correlation detector Axell *et al.* [59] take the maximum value among all the possible time mismatches between the sampling starting time and the OFDM first transmitted sample:

$$Y \triangleq \max_{\tau} \frac{\sum_{i=0}^{N_s+N_{cp}-1} |R_i|^2}{\sum_{k \in S_\tau} |R_k - \frac{1}{N_{cp}} \sum_{k \in S_\tau} \Re\left(R_i\right)|^2 + \sum_{j \notin S_\tau} |R_j|^2} \lessgtr \eta_{GLRT}$$

where S_τ is the set of all possible values of τ for which $x_{i+\tau} = x_{i+N_{cp}+\tau}$.
One can see that no prior knowledge about neither noise nor the signal power level is required, although the authors do not provide any closed form for the distribution of Y and the decision threshold η_{GLRT} must be computed empirically.
In this work we consider as well a second version of the GLRT detector, in which the noise power level is assumed to be known; in this case the detection formula becomes the following simplified one:

$$Y \propto \max_{\tau} \left(\sum_{i \in S_\tau} \Re(R_i) \right)^2 \lessgtr \eta_{GLRT\_UK}$$

In the rest of this paper the GLRT version with unknown parameters will be referred to as *GLRT_UK*, while the GLRT detector with known noise power level will be simply referred to as *GLRT*.

2.3.1.5 Sequential and quickest detection

In [61] authors change point of view on designing cognitive detectors. Instead of minimizing the probability of misdetection given a specific number of samples, Poor *et al.*, based on the theory of sequential analysis firstly introduced by Wald in [62], focused on minimizing the delay on detecting a change in the channel condition.
In cognitive networks, the main goal is to detect precisely and rapidly, the instant in which the user owning the channel, starts or stops transmitting, to best exploit the holes in time in a certain frequency without creating interference. Hence, instead of focusing on avoiding misdetections, the authors design a detector that would be able to quickly detect channel changes in terms of samples statistics.
Every time a new sample is picked up, the quickest detector (*QKDT*) processes all the collected samples and, by using a generalized log-likelihood ratio, it tries to find the most likely moment in which a change in the samples statistics has occurred; if this changes is significant (i.e. greater than a threshold) the channel is stated as busy. A similar reasoning is made to detect the end of transmission i.e. the idle state of the channel.
Assuming $f_{1,P}(x)$ and $f_0(x)$ respectively the Gaussian probability function in the presence of a transmitted signal at power P and in the absence of any transmitted signals, the quickest detector computes:

$$g_t = \max_{k \leq t} \sum_{i=k}^{t} \ln \left(\frac{\sup_P f_{1,P}(x_i}{f_0(x_i)} \right) \lessgtr \eta_{QKDT}$$

where taking the sup_P means finding the received power level that maximize the function $f_{1,P}(x)$ for the given sample x_i.
If, for a given k, g_t is greater than the threshold η_{QKDT} the quickest detector declares the presence of a transmitted signal started at the *k-th* sample.

2.3.2 Detector performances evaluation

For generating the transmission signal we use the QPSK modulation with a coding rate of 1/2, for an overall data rate of 3Mbit/s. We assume this combination of modulation and coding as a typical modulation choice for moving vehicles both in an highway or in a metropolitan scenario.
We evaluate the detectors using two channel models; the channel model mentioned in 2.1.2, even though it has been used as reference by the IEEE 802.11p standard working group, several works have shown that independence among the Gaussian processes generating the parameters for the different taps, is not a valid assumption in vehicular networks. In the model proposed in [63] Matolack et al., after a long and accurate measurement campaign, propose a modified TDL model where the Gaussian processes used to generate taps coefficients are correlated, specifying the correlation coefficients as well. They also introduce a model based on Markov processes to manage the fact that the different taps may appear and disappear at certain time instants: the variability among paths delays is translated in this second model in a birth and death behaviour of the taps. As a consequence, with proper parameters, taps appear and disappear following a Markov birth-death process. For each of the two vehicular channel's model we selected two different scenarios: one is a highway scenario and the other one is a urban environment; in both scenarios vehicles speeds are randomly chosen with a maximum value of respectively 260 km/h and 60 km/h: in fact in highway scenarios, where maximum speed limit is typically about 130 km/h, the relative speed between two incoming vehicles can reach the speed of 260 km/h; on the contrary in urban scenario, especially in an high vehicle density situation, even if maximum speed is about 50 km/h, it's quite difficult to have two oncoming cars cruising at the maximum speed.
For fixed window size detectors, i.e. *ES*, *AC* and both *GLRT* detectors, we choose a number of samples equals to 5 OFDM symbols: the dimension of the IEEE 802.11p short and long training symbols plus the *SIGNAL* symbol which are always present. Five OFDM symbols appears to be the best trade-off between speed and reliability in signal detection as far as the frame length is concerned. In fact, although choosing a large window size, as in Fig. 2.15, allows function $R(i)$ to better state the presence of an OFDM signal, in vehicular networks, a large window size cannot be chosen

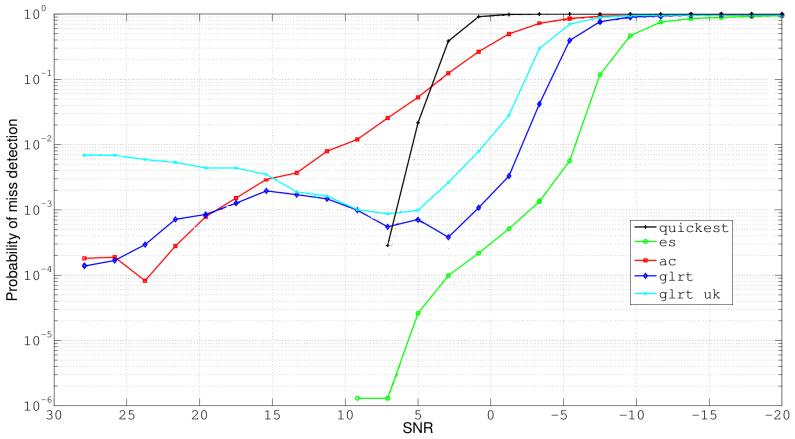

Figure 2.16. *Probability of misdetection in urban scenario with channel model [32]*

since having frames with a big number of OFDM symbols is a pretty rare occurrence, especially when looking at safety messages.
The design parameters for the quickest detector are different. Basically, only two parameter are needed, the probability of false alarm P_{fa} and the average sensing time T_0 before a false alarm can possibly occur (or, in other words, the rate of occurrence, in the average sense, of false alarms).
In our tests we focused on detecting one single transmitted message for different Signal to Noise Ratios. An IEEE 802.11p frame of 250 byte length, typical value for safety messages, is transmitted with a power of 200 mW. Consistently with the noise power level, the signal power is lowered down to reach the desired SNR level; there, the received signal is obtained by filtering the signal with a TDL realization, properly scaled to have average gain of 1.
We focused on two main performance indexes, the probability of misdetection P_{miss} and the detection delay; the probability of false alarm has been used as a design parameter to properly choose the threshold levels; a P_{fa} of 0.01 has been considered as a proper choice.

2.3.3 Results

In figures 2.16 2.17 2.18 and 2.19 the probability of misdetection is shown for the 5 detectors: *ES*, *AC*, *GLRT*, *GLRT_UK* and *QKDT*.

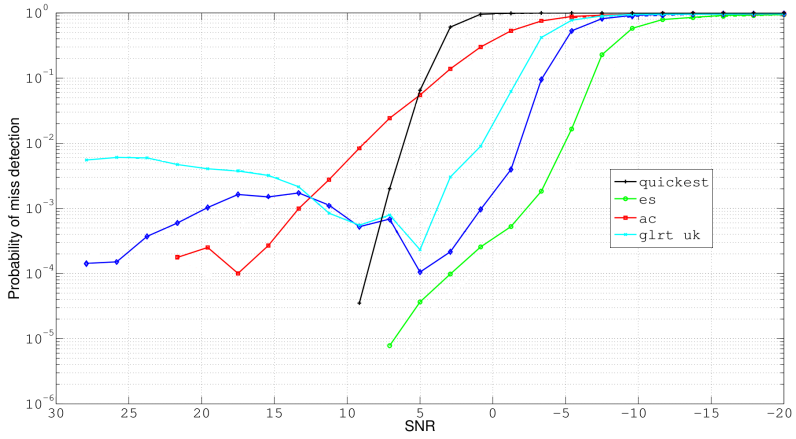

Figure 2.17. *Probability of misdetection in highway scenario with channel model [32]*

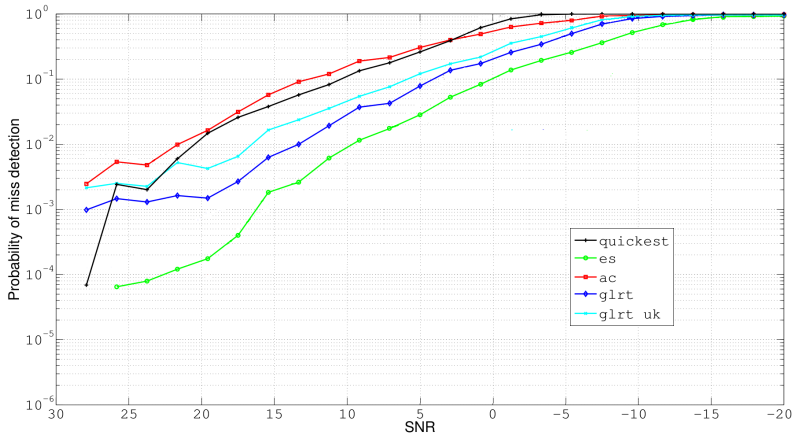

Figure 2.18. *Probability of misdetection in urban scenario with channel model [63]*

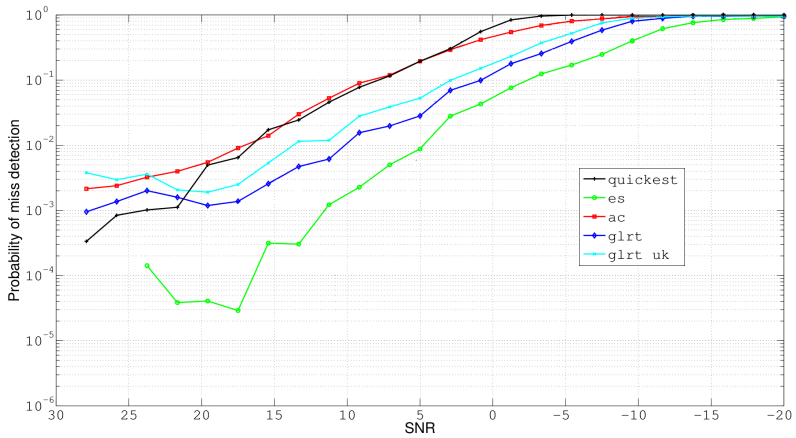

Figure 2.19. *Probability of misdetection in open-area scenario with channel model [63]*

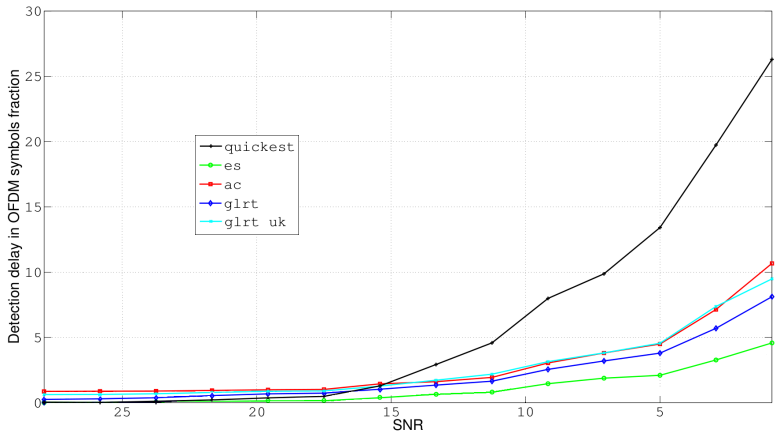

Figure 2.20. *Detection delay in samples, in open-area scenario with channel model [63]*

In the group of fixed window size detectors, apparently the *ES* detector shows the best performances: it exhibits a P_{miss} below 10^{-2} even in near zero SNR conditions. This result is probably due to the length of the observing window, which is too short for exploiting the OFDM second-order characteristics. Authors think that these kind of detectors would exhibit better performance in different scenarios, where channel could be sensed for a longer time, collecting more OFDM symbols.
For high SNRs, the quickest detector shows almost the same results of the energy detector, but, as the SNR decreases, it shows a faster performances decay. This fact is due to the log-likelihood ratio which becomes smaller and smaller as the SNR goes down. In fact, the function g_t of the quickest detector, as the transmission starts, has an increasing trend, whose slope depends on the SNR level. For small values of the SNR, the slope is slightly positive and the quickest detector's function g_t takes more time to cross the threshold.
This delay can be well seen in Fig. 2.20 where the detection delay is represented. In Fig. 2.20 we show the detection delay only for values of P_{miss} below the threshold of 0.5, since it would be meaningless showing a delay for an undetected transmission. It can be seen how, even for fixed observation window detectors, as the SNR decreases, the delay to detect the presence of a signal increases only for vehicular channels.

2.3.4 Final considerations

Taking under examination the most popular cognitive detectors we show the limits of second-order detectors used in vehicular communications, where average messages length are well shorter than data streams usually observed in classical cognitive applications.
The obtained results show that in case of short messages, the fastest and most reliable detector is also the simplest one (i.e. the energy sensing detector), which, without any priori knowledge on transmitted signal modulation, outperforms more complicated detectors that need more informations and assumptions on the transmitted signal.

Chapter 3

5G networks and Wireless Sensor networks

Internet of things (IoT) will be the ideal application for the future 5G networks. Currently IoT networks are isolated clusters of interconnected devices unable to communicated outside the localized area where they are deployed.
5G networks will be the framework capable of providing the seamless connectivity that will finally interconnect these isolated networks and realized the vision of the globally interconnected smart world.
The convergence of wireless sensor network (WSN) and mobile cellular network is not straightforward and some open issue are still present [64].
However, different proposals are all based on the assumption that such low-energy devices will in any case be equipped with more than one radio access interface to exploit both the low-energy consumption WSN protocols such as IEEE802.15.4 or Bluetooth, and the gain in efficiency thanks to a centralized control by the mobile cellular network.
The natural glue for different physical and MAC technologies is the internet protocol (IP) and in particular the new IPv6 protocol [65].
The biggest novelty introduced by IPv6 is the increase in the addressing space which moves from the actual order of 10^9 possible IPv4 addresses to more than 10^{38} IPv6 addresses. Moreover, thanks to this enormous increases in addressing space, the procedures for address self-assignment have been simplified.
However, for low-energy and resource-constrained networks such as wireless sen-

sor networks (WSNs), IPv6 protocol has the drawback of inefficiencies in the transmission, since such large internet addresses significantly lowers the ratio betweeen the payload and the header.
To provide IPv6 internet connectivity to WSNs, IETF provides an adaptation protocol named 6LoWPAN [66], which includes some IPv6 header compression techniques that leverage context sharing and on information retrievable by the lower-layer protocol headers. In the best case scenario, 6LoWPAN could shrink a 40-byte IPv6 header to only 3-bytes long header.
In this section, an innovative implementation of the IPv6 / 6LoWPAN protocol stack is presented. More specifically the principles that have driven the design process are highlighted, pointing out the benefits of the introduced features in the context of WSN, paying particular attention to the novel memory management approach used in the stack, which enables a better support for multi-hop communications, typical of mesh networks like WSNs.
Finally measured performances of the implementation are shown and compared against the most popular IPv6 protocol implementation for low-energy devices named BLIP.

3.1 Related work

In the past decade, Wireless Sensor Network (WSN) research has been more focused on protocol optimization rather than on defining the protocol stack architecture. An effect of this trend has been noticed in the stack implementations, e.g., Levis et al. [67] noted a lack of consensus on the networking abstractions required in TinyOS, a popular open-source operating system for embedded devices. With the aim of defining a networking abstraction, TinyNET [68] provided a networking framework able to support a wide set of protocol interactions and network services, including 6LoWPAN, but traditional layering was still not adopted.
As the IoT concept became more popular, the feasibility of more traditional networking stack architectures have been investigated [69, 70] with the aim of building smart objects using a set of protocols as similar as possible to the ones widely adopted in the Internet. At the same time a number of implementations of the IPv6/6LoWPAN protocol suite have been developed by many institutions. Out of those, the most

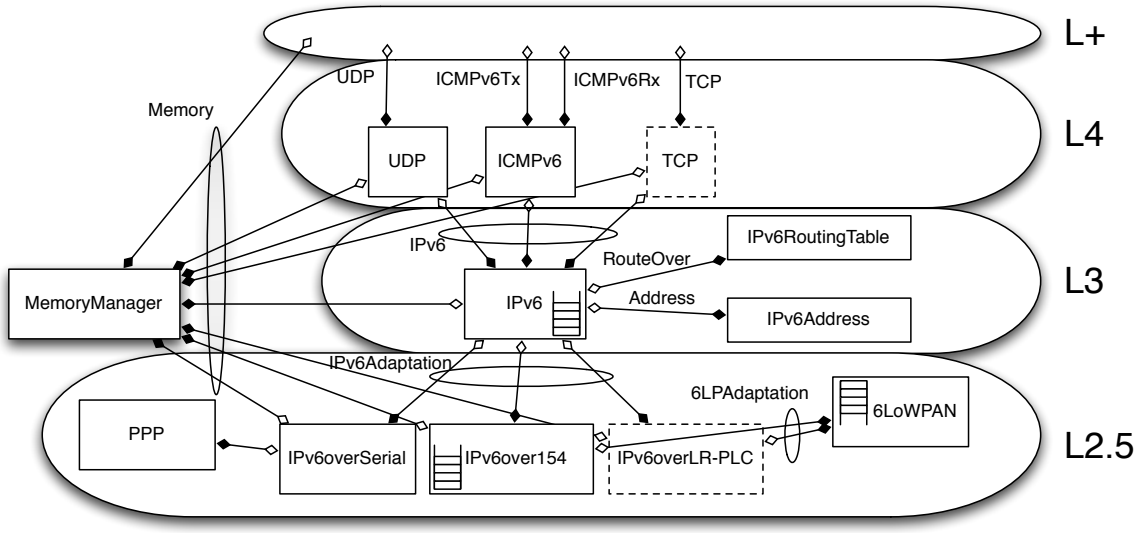

Figure 3.1. *SiGLoWPAN architecture*

popular open-source implementations [71] are BLIP for TinyOS, and uIPv6 for Contiki.

As previously mentioned the integration of wireless sensor networks within the global internet network is inevitable, however, the IP stack should be carefully designed to be easily portable to different physical layers, flexibly support IP layer routing (e.g., RPL [72]), handle concurrent communications, and fulfil strict memory requirements posed by the WSN scenario.

3.2 SiGLoWPAN implementation

3.2.1 Requirements and design goals

Since a large number of different transmission technologies, are involved in current WSNs, and moreover 5G support will likely be added, an IP stack implementation suitable for this scenario has to properly address the technical difficulties that may arise from such a complex networking infrastructure. This goal is even more challenging if we keep in mind that almost all WSN devices are cheap hardware-constrained nodes which can handle only a very limited set of networking protocols.

With the aim of addressing such requirements, the design of SiGLoWPAN was driven by the following goals.

3.2.1.1 Effective layer-3 routing

Given the very wide range of medium access technologies that are involved, the requirement of effective routing support on top of different link-layers is a key objective for SiGLoWPAN. Even if other implementations already support L3 routing, the chosen architectural design and in particular the advanced memory management approach spanning from the lower layers up to the application allows SiGLoWPAN to efficiently handle relaying operations even on very constrained devices with few kilobytes of RAM and limited computing resources.

3.2.1.2 Link-layer independence

Motivated by the same consideration about the number of PHY layers upon which future WSNs will be built, the modules composing SiGLoWPAN have been carefully selected with the intent to achieve a cleanly layered implementation, possibly maintaining one-to-one correspondence between a protocol and the module where it is implemented. Thanks to this flexible but clean modularization, which confines each protocol within a single component, a high-level of flexibility and code reuse has been possible in this complex stack implementation, which supports 6LoWPAN independently from a specific link-layer and point-to-point protocol (PPP) communication over the serial link.

3.2.1.3 Lightweight implementation

The constrained nature of the majority of the devices involved in IoT scenarios, imposes hard limits on the number of instructions per second and the amount of memory that a device can afford. Although the efficiency of the implementation initially had lower priority with respect to the other objectives previously discussed, a careful evaluation of the design choices made it possible to pursue this requirement as an additional goal. Thanks to the clean modularization, and by maximizing the level of code reuse, SiGLoWPAN implements the whole set of protocols using a small fraction of the ROM resources available on a realistic 16-bit RISC MCU

(i.e., MSP430). On the same platform, the aforementioned memory management approach leads also to a very efficient RAM allocation. As a consequence, this efficient resource usage has become a key feature, and allows the system to allocate more memory to the small IP queues, which are typical of constrained devices, thus directly improving the transmission and relaying performance network-wide.

3.2.2 Architectural overview

As discussed in the previous paragraphs, and shown in Fig. 3.1, the SiGLoWPAN architecture is clearly layered and organized in self-contained modules corresponding to single protocols. As an exception, the memory management module spans across all the networking components up to the highest application layer of the node (denoted in Fig. 3.1 as L+). Besides the well-known layers 3 and 4, Fig. 3.1 also shows the IP adaptation layer (i.e., layer 2.5) that performs the adaptations required to transport IP packets over specific link-layers.
From a high-level perspective, SiGLoWPAN gives the application layer access to the IPv6 stack by means of the TinyOS interfaces of the layer 4 protocols, such as `UDP`, `ICMPv6Rx` and `ICMPv6Tx`. Different instances of such interfaces are present, allowing multiple components to be linked to the same protocol; multiplexing is obtained using protocol parameters such as the local UDP port, e.g., an L+ application will setup UDP listening by linking to a specific instance of `UDP` interface identified by the local UDP port number.
The architecture proposed in Fig. 3.1 is *memory-centric* because of the centrality of the `MemoryManager` component, which is shared from the lower layer 2.5, up to the application layer of the stack. This design choice is motivated by the consideration that every component not using the `MemoryManager` must allocate a static buffer. The problem is that such a static buffer must be big enough to accommodate the maximum data which could be supported by this component, leading to memory usage inefficiencies inside the application components. Since IPv6 MTU is 1280 bytes, in real-life applications a single datagram may represent a considerable fraction of the available RAM on constrained devices (e.g., telosb has 10kB of RAM). In addition, when a datagram is statically allocated at L+, lower layers have to either fully process it immediately or duplicate it in RAM for delayed processing,

which always results in some kind of inefficiency. Moreover, for datagrams received for forwarding, tighter requirements apply on immediate processing or duplication, thus dynamic memory management becomes the only feasible choice to efficiently handle the transmission chain across the stack, especially when concurrent routing of multiple IP datagrams is required.
Link-layer independence is another important design goal of SiGLoWPAN. In order to meet this requirement, the design of adaptation layers has been carried out in a highly modular fashion. IPv6 module handles a set of IPv6 adaptation layers using the `IPv6Adaptation` interface. Modules providing such interface have to offer the capability to transmit or receive IP datagrams over a specific medium, one at a time. The 6LoWPAN header compression and fragmentation approach has been implemented in a separate module, shared across the subset of adaptation layers supporting such compression (i.e., IEEE 802.15.4, LR-PLC, BT-LE [73], etc.). Unconstrained media that do not require such a kind of adaptation may use other techniques, i.e., serial communication with a PC has been implemented using PPP.
Apart from the IP layer routing, SiGLoWPAN provides the capability to perform layer 2 routing (*mesh-under*) through the `MeshUnder` interface available at layer 2.5.
The initial planning of SiGLoWPAN, started identifying which would have been the specific objectives to target to. First of all, two areas where optimizations could be performed have been identified: *memory management* and *architectural design*. It is well-known that TinyOS, one of the principal operative systems (OS) for low-power devices, does not allow dynamic memory allocation. This is a very limiting factor when dealing with IP, because dynamic memory can save from pre-allocating memory which could be unneeded and thus wasted. For this reason, the first improvement of SiGLoWPAN has been to define a RAM manager module that manages RAM among modules and the application running on a node (see Fig. 3.1). The *Memory* manager component has been designed to provide classic RAM handling functions, like *alloc* and *free*, and also some network protocols-oriented functions, like *realloc* and *hrealloc*, which can add or remove space in both head or tail of a buffer. The two latter functions are very useful when dealing with headers and footers.
Another goal in SiGLoWPAN is achieved with a clear layer design, avoiding to implement modules including more than one protocol, still attaining the code weight-

lessness: using the fewest possible function calls, sharing the fewest possible parameters. Avoiding to implement modules including more than one protocol, SiGLoWPAN achieved the second goal: a clear, simple and modular layer design. Anyway, the modular architecture has been obtained still keeping low the memory burden of the code, using the fewest possible function calls, sharing the fewest possible parameters. Moreover, to allow future updates, as well as to extend portability to other platforms and OSs, all protocol-dependent functions have been encapsulated within generic header files (Table 3.1).

3.2.3 Components

The SiGLoWPAN stack is composed of both TinyOS modules and reusable standard C files, which are described in Table 3.1.

Table 3.1. *List of SiGLoWPAN header files*

6LOWPAN.h	IPv6 packet format definitions
RFC4944.h	fragmentation header structure definition, mesh-under header structure definition
RFC6282.h	LOWPAN_IPHC header structure definition, LOWPAN_NHC structure definition
RFC4944.c	fragmentation handling functions, mesh-under header handling functions
RFC6282.c	LOWPAN_IPHC handling functions, LOWPAN_NHC handling functions

The set of TinyOS modules forming SiGLoWPAN are shown in Fig. 3.1. The main components will be briefly described in the following.

3.2.3.1 `MemoryManager`

The `MemoryManager` component has a paramount relevance. Though this module has been designed as a general purpose memory allocation component, it is currently only involved in handling the buffer space required for IPv6 datagrams.
At compile time, a fraction of the available RAM of the node is statically allocated

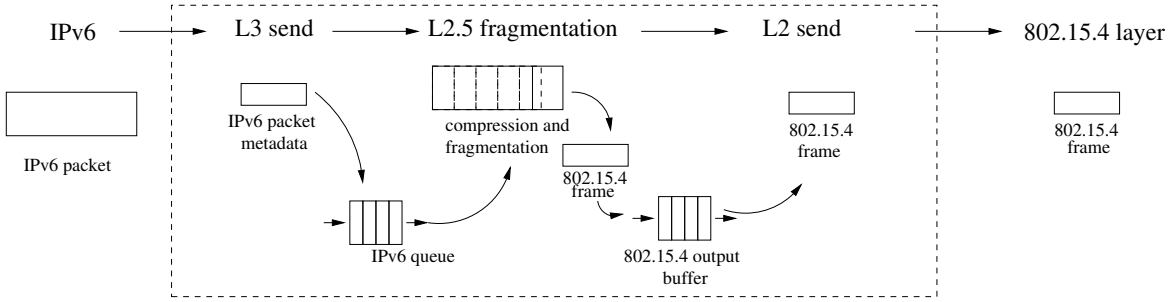

Figure 3.2. *SiGLoWPAN sending procedure workflow*

to this component, which will be assigned to the modules that need it by means of the *alloc* call. In order to enable complex interactions with buffer spaces, the memory manager makes the available RAM virtual by identifying each specific allocation using a virtual memory ID (`vmID`) rather than a physical memory address. The pointer to the physical address is obtained using the *id2p* call.

RAM virtualization enables transparent reallocation of the buffer space, which is especially useful in optimizing RAM requirements for single datagrams along the whole network stack. In fact, `vmID` is a global identifier for the buffer space and can be passed between layers removing the need for static memory allocations.

This process is managed using the header reallocation feature of the buffer through the *hrealloc* call. This function resizes the buffer by changing the physical address of the first byte and thus makes it possible to transparently add or remove headers to a buffer space.

When a packet is to be sent, at each layer of SiGLoWPAN the first part of the buffer is moved backwards and filled with the corresponding layer header, then only the `vmID` is signaled to the next layer. Network modules may also remove headers by calling the function *hrealloc* requesting a negative header reallocation on the buffer. The reallocation procedure is performed by the `MemoryManager`, by leveraging the fact that its memory pool is assigned starting from the bottom, the *hrealloc* procedure is simple and involves only memory pointer arithmetic without requiring any memory copying operation.

3.2.3.2 L2.5

Layer 2.5 is the lowest level of the SiGLoWPAN stack, and performs the adaptation required to transmit IPv6 datagrams over a specific network interface. As the corresponding IP-over-X IETF specification, these modules can be either sim-

ple or complex depending on what are the operations required in order to adapt IPv6 packets for transmission on a specific L2 frame format. Modules at this layer receive a datagram to be transmitted as well as the next-hop target from the IPv6 component. As soon as the adaptation module is ready to receive a new datagram, it notifies IPv6 of this status by signalling a *sendDone* event.

The design of the `6LoWPAN` component required a more careful consideration in order to get a high level of code reuse across the different link-layer drivers. For this purpose, the interactions of `6LoWPAN` with actual layer 2.5 components occurs through the *6LPAdaptation* interface, which provides compression and fragmentation procedures for transmission, and their counterparts for reception. Each module using the *6LPAdaptation* interface offloads the operations required to build and process L2 frames to `6LoWPAN`.

Fig. 3.2 shows from a high level perspective the workflow performed during the send operation of an IPv6 datagram over IEEE 802.15.4 (6LoWPAN). As soon as the datagram to be sent is received by the `IPv6over154` component, the datagram and the data-link layer specific metadata required to compress the packet are passed to the `6LoWPAN` component using the *compress* command of the *6LPAdaptation* interface; the *compress* command builds a single L2 frame of the datagram at every call. As long as the `IPv6over154` has available slots in its internal output frame buffer, all the 6LoWPAN fragments are built subsequently; otherwise the remaining fragments will be built after each successful transmission.

The receive procedure is very similar, each unprocessed L2 frame is passed to the `6LoWPAN` component which will reconstruct the IPv6 datagram. As soon as the IPv6 datagram is fully reconstructed, it is passed to the corresponding adaptation layer module using the *6LPAdaptation* interface. This approach makes it possible to use a single queue to store the datagrams during the reconstruction phase. This queue is shared among the whole set of adaptation modules.

`IPv6over154` statically allocates a pool of L2 frames to hold the processed fragments waiting for transmission as well as the unprocessed fragments waiting for reconstruction. In our implementation the buffer space is shared for both the transmission and reception queues.

3.2.3.3 L3

The layer 3 of our IPv6 stack is composed of the `IPv6` module and its companion modules, i.e., `IPv6Address` and `IPv6RoutingTable`.
The `IPv6` component is characterized by the following features: i) it provides *send* and *receive* primitives to the upper layers, ii) it keeps track of the available link-layer interfaces and their operational state, iii) it keeps track of the local IPv6 addresses along with `IPv6Address`, iv) it performs routing operations and decisions on each IPv6 datagram together with `IPv6RoutingTable`, and v) it provides IPv6 pseudo-header support to enable upper-layer protocols to perform checksum calculations.
For each datagram `IPv6` *puts in* or *pops out* the IPv6 header from the corresponding buffer space, leveraging the *hrealloc* function, and thus without any additional memory allocation.
Each datagram received by the IPv6 layer, either from the network or from the upper layers, passes through the routing engine which either i) delivers it locally if its destination corresponds to the local node, ii) flags it to be routed towards a specific link-local next-hop of an active adaptation interface, or iii) silently discards it.
The local delivery procedure is performed by querying the `IPv6Address` component to understand whether the target IPv6 is the local node. This component maintains a list of all the local IPv6 addresses, keeping track of the name and type of the interface associated to each address. The classification type of the interface depends on the address characteristics, i.e., unicast or multicast, global, site-local or link-local. The `IPv6Address` component is also used to assign a source IPv6 address to each locally outgoing datagram. The routing procedure is assisted by the `IPv6RoutingTable` component, that is queried for the next-hop node, once the IPv6 destination of the datagram is given. This component maintains a table containing the next-hop host for every particular IPv6 prefix known by the local node. In order to simplify the prefix matching process, which could take a considerable amount of time, entries are kept sorted using the destination prefix length field, from the longest to the shortest.

Table 3.2. *SiGLoWPAN ROM and RAM expressed in bytes*

Component	ROM (B)	RAM(B)
TinyOS & CC2420 transceiver	10714	383
`MemoryManager`	1002	6996[1]
L2.5: `6LoWPAN` & `IPv6over154`	7176	1904
L3: all	2572	956
L4: `UDP`	130	-
Total	21594	10239
Free space	*27558*	*6994*

3.2.3.4 L4

Layer 4 is composed of the modules typically used by the application layer. Currently only `UDP` and `ICMPv6` is provided, but additional protocols can be easily added to the stack by implementing a specific protocol on top of the `IPv6` module. The `UDP` module handles UDP datagrams, i.e., IPv6 datagrams containing the UDP next-header received by the node delivered by `IPv6`. This delivery process is implemented leveraging static linking of TinyOS by means of parametrized interfaces. The same applies to `ICMPv6`.
Thanks to the RAM manager, when an L4 packet is sent, each module reallocates the buffer and adds the proper header on top of it. Analogously, when a packet is received, the module extracts the header information and deallocates the buffer memory pertaining to the header, without any additional RAM requirement inside the L4 component.

3.3 Evaluation

An experimental evaluation campaign has been performed using our SiGLoWPAN implementation to show i) its RAM and ROM memory footprint, and ii) the achievable throughput at layer 4 compared to another 6LoWPAN implementation, i.e., BLIP.

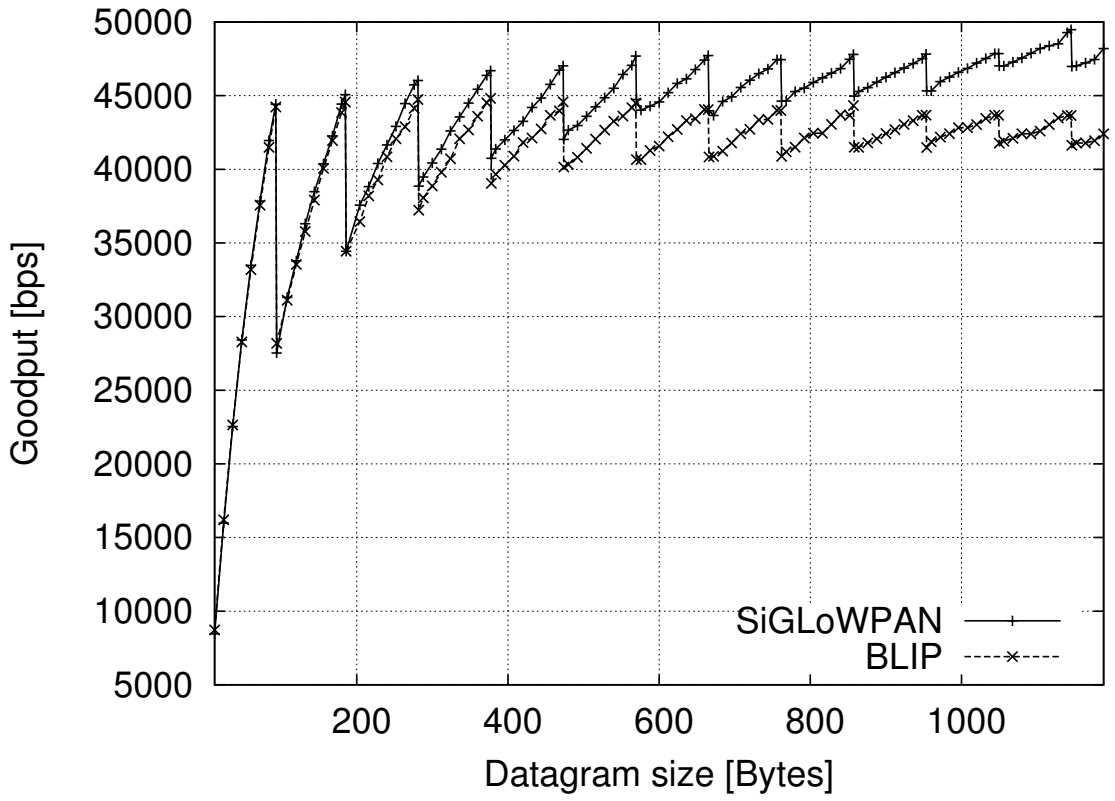

Figure 3.3. *Receive-side goodput comparison between BLIP and SiGLoWPAN*

Table 3.2 shows the overall ROM and RAM allocations across the different components of the stack. In the proposed experiment the `MemoryManager` offers 6170 bytes of RAM to the components, `IPv6RoutingTable` holds up to 20 entries, `IPv6` queue is 10 datagrams long, `IPv6over154` can queue up to 12 IEEE 802.15.4 frames, the `6LoWPAN` reconstruction queue is 10 IPv6 packets long and the application at layer L+ can send packets of arbitrary size up to 1240 bytes of payload.
It can be noted that more than two-thirds of the RAM is allocated to the Memory component and the remaining third is mainly split between L2.5 and L3 components. The memory assigned to the 6LoWPAN components is mainly used to allocate the L2 output frame buffer, but also to hold metadata required for fragmented IPv6 datagrams reconstruction; the RAM allocated to layer 3 is mainly used to store the routing table but also for the metadata required by IP layer queuing. This result highlights the memory efficiency of the implementation that makes it possible to

[1]Unused RAM is assigned to the `MemoryManager`. This value includes 6994 bytes of free RAM available and dynamically allocable by L+ components.

assign the biggest part of the node resources to network buffers and IP routing.
Table 3.2 shows the amount of ROM required for program code of the various SiGLoWPAN subsystems; the grand total of ROM occupied by SiGLoWPAN is 11kB, required mainly by the 6LoWPAN header compression and fragmentation handling functions. This result motivates the introduction of our reusable 6LoWPAN component shared across the different network interfaces using this compression. ROM occupancy is about 2kB less than BLIP, even though a detailed comparison is not possible because there may exist minor differences in the implemented features that have an impact on the program size; for example SiGLoWPAN includes a more complex `MemoryManager` component supporting hrealloc, whereas BLIP has a simpler and hence smaller one.
To test the throughput of the whole protocol stack, an application implementing the Iperf [74] protocol has been developed over both SiGLoWPAN and BLIP measuring the goodput of an UDP unicast constant bitrate (CBR) session.
Figure 3.3 shows a comparison between SiGLoWPAN and BLIP. The experiment measured the goodput at the receiver between two telosb [75] nodes on the same IEEE 802.15.4 PAN within range of each other; to this end the client node starts a UDP CBR session towards the server which measures the average speed at which the data at the L+ layer is received. To perform a fair comparison between BLIP and SiGLoWPAN, all the comparable network buffers in the two implementations have been set to the same length. It has been proved that the bottleneck was at the client side for both BLIP and SiGLoWPAN, which were unable to send the IPv6 datagrams faster than the speed shown, whereas at the receiver side the packet loss was negligible. Very small datagrams experience slow throughput due to the high fixed time required to successfully emit an L2 frame, the overhead added by the 6LoWPAN header, and its complex compression process.
The sawtooth-like pattern in the graph is due to the reduced efficiency caused by the introduction of an additional L2 frame required to transmit an IPv6 datagram when its last fragment grows exceeds the L2 frame MTU.
SiGLoWPAN outperforms BLIP for larger datagrams up to 13%, mainly due to the fact that BLIP fragments an IPv6 datagram at the 6LoWPAN layer in a single step, thus requiring that the L2 queue has enough space for all the fragments at once. SiGLoWPAN can build the datagram in successive steps, thanks to the advanced

memory system supporting the *hrealloc* function that does not require static allocation at the L+ layers and makes it possible to perform the *free* operation at the lowest layers of the stack.

3.4 Final remarks

The IPv6 / 6LoWPAN stack implemented, introduced innovative principles for protocol implementations and memory management for resource-constrained devices. This architectural design allows smoother implementation and integration of data-link protocol. Moreover experimental evaluations highlighted the benefits in terms of point-to-point throughput introduced by the adopted cross-layer optimization of the protocol stack.

Chapter 4

5G and green communications

Machine type communications include different kinds of applications, each with different requirements about the network connection service, that 5G will have to meet.

Applications like remote monitoring will likely need to transport large amount of video streaming data and hence it will require a sufficient level of always-available bandwidth to deliver video data; while applications for industrial remote controls are based on sharing messages that must be delivered within very short and deterministic time.

In applications for smart metering, like in wireless sensor networks, the main concern is about devices' life. The cost of manually place devices is typically orders of magnitude higher than the actual cost of the devices themselves, thus making them last as long as possible is one of the main objectives.

Moreover in recent years, the increasing awareness in energy consumptions as principal cause of global warming, has focused the attention in developing communication protocols with a special care on energy efficiency.

In wireless devices, a considerable quantity of energy is spent in transmissions.

Many proposals have been presented for reducing transmission power. Here we focus on transmission power allocation to subsequent retransmissions for protocols that adopts hybrid automatic repeat request (HARQ) techniques, like for example in current 4G networks.

HARQ techniques jointly exploit a Forward Error Correction (FEC) code and an Automatic Repeat reQuest retransmission process to increase the throughput of the

communication. HARQ processes can be divided in two categories:

1. Type-I HARQ processes, in which, for every transmission attempt, the destination discards the received packet if decoding fails;

2. Type-II HARQ processes, in which, previously received versions of the packet are combined before trying to decode the message.

In particular, we can further distinguish two kinds of Type-II HARQ processes, i.e.,

1. Chase Combining (CC) HARQ, in which the entire codeword is sent in each transmission attempt;

2. Incremental Redundancy (IR) HARQ, in which the original codeword is divided into multiple sub-codewords that are sent in successive transmission attempts.

Despite the works presented in [76, 77], [78] and [79], we use the novel theory of code rate in finite block-length regime [80], in which the Shannon coding theory [81] is revised to eliminate the assumption of the asymptotic regime.
From the information theory, the capacity of a communication channel is defined as the maximum value of the mutual information I between the channel input x and the output y over the margin distribution of x p_x, i.e., $C = \max_{p_x} I(x;y)$. The Shannon theory states that in additive white Gaussian noise (AWGN) channels , where the noise w has a Gaussian distribution with mean $\mu = 0$ and variance σ_w^2, the output value y is given by $y = x + w$ and, therefore, it is Gaussian conditioned to the value of x, i.e., $p_{y|x}(y|x) \sim \mathcal{N}(x, \sigma_w^2)$. In this case, the channel capacity is reached for Gaussian distributed input values of x, i.e., $x \sim \mathcal{N}(0, \sigma_x^2)$. The value of channel capacity is given by

$$C = \frac{1}{2}\log_2\left(\frac{\sigma_y^2}{\sigma_w^2}\right) = \frac{1}{2}\log_2\left(1+\Gamma\right) \text{ [bpcu]} \tag{4.1}$$

where $\sigma_y^2 = \sigma_x^2 + \sigma_w^2$ and $\Gamma = \sigma_x^2/\sigma_w^2$ is the Signal-to-Noise Ratio (SNR). In the case of passband transmission, since we are dealing with two parallel AWGN channels, the capacity is doubled: $C = \log_2(1+\Gamma)$ bpcu.
However, recent studies by Polyanskiy-Poor-Verdú [80] provide interesting results

on the finite block-length regime, i.e., for a scenario in which the length of codewords is constrained, linking the Shannon channel capacity, transmission rate, and decoding error probability.

Here we extend the work presented in [82] where authors investigate the performance of Type-I HARQ processes in the context of finite block-length regime. They seek the optimum power allocation over successive transmission attempts that minimizes the outage probability, i.e., the probability that the packet can not be correctly delivered after M transmissions, under a constraint on the average transmit power $\bar{P}$. Their results basically show that transmission power increases at each transmission attempt. In our work, instead, we are interested in analysing the gain provided by combining previously received copies of the transmitted packet at the receiver side in the context of finite block-length coding. In particular, we want to provide a novel comparison between the performance of CC HARQ and IR HARQ processes in the finite block-length regime communication. In the literature, to the authors' best knowledge, CC HARQ processes in the finite block-length regime have not been addressed yet. IR-HARQ processes, instead, have been studied in [83], but the proposed analytic expressions cannot be used in our context as we assume that the coherence time of the wireless channel is shorter than the length of the transmission round.
The remainder of the chapter is organized as follows. In Section 4.1 the system model and the optimization problem are outlined. In Section 4.2 the performance of Type-I, CC-HARQ, and IR-HARQ is compared and some considerations about energy consumption are made. Finally, in Section 4.3 we draw the conclusions and point out the future work on this topic.

4.1 System Model

Consider a HARQ system based on a finite block-length code [80]. Assume that every transmitted symbol is taken from the alphabet $\mathcal{M}$ and b information symbols are encoded into a codeword belonging to the set $\mathcal{M}^L$, i.e., a codeword taking L

channel uses to be transmitted. The codeword rate is, then,

$$R = \frac{\log_2 |\mathcal{M}|^b}{L} = b \cdot \frac{\log_2 |\mathcal{M}|}{L} = \frac{b}{L} \text{ bpcu} \tag{4.2}$$

under the assumption of binary symbol alphabet, i.e., $|\mathcal{M}| = 2$. Note that with b bits we can represent $N \triangleq 2^b$ distinct messages. We consider an AWGN channel with complex normal fading coefficients h, whose amplitude $|h|$ is Rayleigh distributed. For the sake of simplicity and without loss of generality, we assume that:

1. the fading process is flat on every transmitted codeword and fading realizations are independent among different blocks;

2. the average value of the squared fading amplitudes $g = |h|^2$, which are exponential random variables, is $\lambda = 1$;

3. the noise has unit power, i.e., $\sigma_w^2 = 1$.

The block scheme of the channel is depicted in Fig. 4.1. Let us denote with P the power of the transmitted symbol and with ϵ the decoding error probability. The results in [80] ensure that there is a coding/encoding procedure (which we assume to use in the following part of the chapter) such that the relationship among transmission rate, Shannon capacity, and error probability is given by

$$R = C - \sqrt{\frac{V}{L}} \cdot Q^{-1}(\epsilon) + \frac{1}{2} \cdot \frac{\log_2 L}{L} + \mathcal{O}(1) \tag{4.3}$$

where $C = \frac{1}{2}\log_2(1+\Gamma)$ bpcu is Shannon capacity, V is defined as *channel dispersion* and is equal to

$$\begin{aligned} V &= \frac{1}{2} \cdot \frac{\Gamma(\Gamma+2)}{(\Gamma+1)^2} (\log_2 e)^2 \\ &= \frac{1}{2} \cdot \left[1 - \frac{1}{(\Gamma+1)^2}\right] (\log_2 e)^2 \end{aligned} \tag{4.4}$$

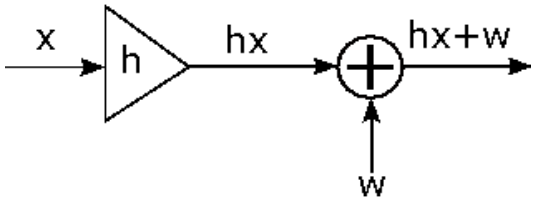

Figure 4.1. *Block scheme of the wireless channel.*

and, as usual, $Q(x) \triangleq (1/\sqrt{2\pi}) \cdot \int_0^\infty e^{-x^2/2}\, dx$. In the case of passband channel Shannon capacity and channel dispersion must be multiplied by two. Therefore, given the values of L, R, P, and the statistics of the fading process g, we can approximate the decoding error probability as

$$\begin{aligned} \phi &\approx \mathbb{E}_g[\epsilon(L,R,gP)] = \\ &= \mathbb{E}_g\left[Q\left(\frac{\sqrt{L}\left(\log_2(1+gP)+0.5\frac{\log_2 L}{L}-R\right)}{\sqrt{1-\frac{1}{(1+gP)^2}}\log_2 e}\right)\right] \end{aligned} \tag{4.5}$$

where $\mathbb{E}$ is the expectation, which is taken on the channel gain value g.

Let M denote the maximum number of transmission attempts, P_m the transmission power employed in the m-th transmission, and Φ_m the probability that the data is not correctly decoded until the m-th transmission attempt. By definition, it is always $\Phi_0 = 1$. We define the average consumed energy as

$$\bar{\xi} = L \cdot \sum_{m=1}^{M} P_m \cdot \Phi_{m-1} \tag{4.6}$$

and the expected number of channel uses, i.e., the average delay as

$$\bar{\tau} = L \cdot \sum_{m=1}^{M} \Phi_{m-1} \tag{4.7}$$

Then, the average transmission power can be obtained using the renewal reward theory, obtaining

$$\bar{P} = \frac{\bar{\xi}}{\bar{\tau}} = \frac{\sum_{m=1}^{M} P_m \cdot \Phi_{m-1}}{\sum_{m=1}^{M} \Phi_{m-1}} \tag{4.8}$$

In[82] the power allocation for successive transmission attempts $\{P_m\}_{m=1}^{M}$ is optimized in order to minimize the outage probability Φ_M, i.e, the probability of packet decoding failure after M transmission attempts, under a constraint on the average transmitted power value.

Here we design a similar optimization problem to investigate which is the performance gap between Type-I HARQ, CC HARQ, and IR HARQ processes. The minimization problem is the following:

$$\begin{aligned} \min_{P_m} \quad & \Phi_M \\ \text{subject to} \quad & \bar{\xi} = J \\ & P_{\min} \leq P_m \leq P_{\max} \end{aligned} \tag{4.9}$$

Note that we are forcing the transmit power P_m in the interval $[P_{\min}, P_{\max}]$, which is a common constraint for a real device. This yields a lower bound $J_{\min}$ and an upper bound $J_{\max}$ on the average consumed energy $\bar{\xi}$. Indeed, $J_{\min}$ is obtained as

$$\begin{aligned} \bar{\xi} &= L \cdot \sum_{m=1}^{M} P_{\mathrm{m}} \cdot \Phi_{m-1} \geq L \cdot \sum_{m=1}^{M} P_{\min} \cdot \Phi_{m-1} \\ &\geq L \cdot P_{\min} \triangleq J_{\min} \end{aligned} \tag{4.10}$$

recalling that $\Phi_0 = 1$. A similar reasoning is applied for the upper bound $J_{\max}$:

$$\begin{aligned} \bar{\xi} &= L \cdot \sum_{m=1}^{M} P_{\mathrm{m}} \cdot \Phi_{m-1} \leq L \cdot \sum_{m=1}^{M} P_{\max} \cdot \Phi_{m-1} \\ &\leq L \cdot P_{\max} \cdot M \triangleq J_{\max} \end{aligned} \tag{4.11}$$

4.1.1 Type-I HARQ

In the case of Type-I HARQ, where the receiver tries to decode only the last received packet discarding previously received information, it is

$$\Phi_m^{(\mathrm{TI})} = \begin{cases} \prod_{j=1}^{m} \phi_j & \text{if } m \neq 0 \\ 1 & \text{if } m = 0 \end{cases} \tag{4.12}$$

where ϕ_j is the probability that the data is not decoded during the j-th transmission attempt, i.e., $\phi_j = \mathbb{E}_g[\epsilon(L, R, gP_j)]$.

4.1.2 CC-HARQ

Now, consider a receiver which collects the replicas of the received packet in a buffer and combines them to increase the effective SNR, i.e., a CC HARQ process. The combination of the packets is done exploiting Maximal Ratio Combining (MRC) [84]. The effective SNR after the j-th transmission attempts is

$$\Gamma_j^{(\mathrm{CC})} = \sum_{\alpha=1}^{j} \Gamma_\alpha = \sum_{\alpha=1}^{j} \frac{g_\alpha P_\alpha}{\sigma_w^2} \tag{4.13}$$

In this context, the decoding error probability at the j-th transmission attempt $\phi_j^{(\mathrm{CC})}$ is expressed as

$$\begin{aligned}\phi_j^{(\mathrm{CC})} &= \mathbb{E}_{g_1,\dots,g_j}\left[\epsilon\left(L, R, \sum_{\alpha=1}^{j} g_\alpha P_\alpha\right)\right] = \\ &= \underbrace{\int_0^{+\infty}\cdots\int_0^{+\infty}}_{j \text{ integrals}} \epsilon\left(L, R, \sum_{\alpha=1}^{j} g_\alpha P_\alpha\right) e^{-\sum_{\alpha=1}^{j} g_\alpha}\, d\mathbf{g}\end{aligned} \tag{4.14}$$

where we exploited the hypothesis of independent block fading process, factoring $f_{g_1,\dots,g_j}(g_1,\dots,g_j)$ as

$$\begin{aligned}f_{g_1,\dots,g_j}(g_1,\dots,g_j) &= f_{g_1}(g_1)\cdots f_{g_m}(g_m) \\ &= e^{-\sum_{i=1}^{m} g_i}\end{aligned} \tag{4.15}$$

The outage probability at the m-th transmission attempt in this case becomes

$$\Phi_m^{(\mathrm{CC})} = \begin{cases}\prod_{j=1}^{m} \phi_j^{(\mathrm{CC})} & \text{if } m \neq 0 \\ 1 & \text{if } m = 0\end{cases} \tag{4.16}$$

4.1.3 IR-HARQ

In this case the original codeword that takes L channel uses to be transmitted is divided into L/M sub-codewords, where M is the maximum number of transmission attempts. We can model this scenario with a M-parallel AWGN channel [85] with Rayleigh fading. In this context Eq. (4.3) becomes

$$R_j = C_j - \sqrt{\frac{V_j}{L/M}} \cdot Q^{-1}(\epsilon) + \frac{1}{2} \cdot \frac{\log_2 L/M}{L/M} + \mathcal{O}(1) \tag{4.17}$$

where C_j is defined as

$$C_j = \sum_{\alpha=1}^{j} C\left(g_\alpha P_\alpha\right) \ , \tag{4.18}$$

i.e., C_j accounts for the cumulative channel capacity, and V_j is equal to

$$V_j = \sum_{\alpha=1}^{j} V\left(g_\alpha P_\alpha\right) \ , \tag{4.19}$$

i.e., V_j accounts for the cumulative channel dispersion. We recall that $\{P_\alpha\}_{\alpha=1}^{j}$ and $\{g_\alpha\}_{\alpha=1}^{j}$ are the transmitted powers and the channel gains employed until transmission attempt j, respectively.

R_j is the information rate after the j-th transmission attempt. Assuming that the mother-code rate of the FEC code is $R = b/L$ (see Eq. 4.2), the code rate of the j-th transmission attempt is defined as

$$R_j = \frac{b}{j \cdot \frac{L}{M}} = R \cdot \frac{M}{j} \tag{4.20}$$

Note that $R_M \equiv R$.

The error probability can be obtained from Eq. (4.17):

$$\epsilon_j^{(\mathrm{IR})} \approx Q\left(\frac{C_j + 0.5\frac{\log_2 L/M}{L/M} - R_j}{\sqrt{V_j/\frac{L}{M}}}\right) \tag{4.21}$$

Therefore, the decoding error probability at the j-th transmission attempt $\phi_j^{(\mathrm{IR})}$ is expressed as follows:

$$\begin{aligned}\phi_j^{(\mathrm{IR})} &= \mathbb{E}_{g_1,\ldots,g_j}\left[\epsilon_j^{(\mathrm{IR})}\right] = \\ &= \underbrace{\int_0^{+\infty} \cdots \int_0^{+\infty}}_{j \text{ integrals}} \epsilon_j^{(\mathrm{IR})} \cdot e^{-\sum_{\alpha=1}^{j} g_\alpha}\, d\mathbf{g}\end{aligned} \tag{4.22}$$

where we exploited again Eq. (4.15).

The outage probability at the m-th transmission attempt in this case becomes

$$\Phi_m^{(\mathrm{IR})} = \begin{cases} \prod_{j=1}^{m} \phi_j^{(\mathrm{IR})} & \text{if } m \neq 0 \\ 1 & \text{if } m = 0 \end{cases} \tag{4.23}$$

4.2 Performance Evaluation

Numerical evaluations have been performed in Matlab®, using the parameters summarized in Table 4.1. Two very short block-lengths, i.e., $L \in \{50, 200\}$, and just $M = 2$ transmission attempts have been considered, in order to reduce the amount of buffering required to support data retransmission, which is a really important constraint for cost- and latency-sensitive MTDs [86].

Table 4.1. *Simulation parameter list.*

Parameter	Value
$P_{\min}$	0 dB
$P_{\max}$	20 dB
L	$\{50, 200\}$
R	1.44 bpcu
M	2

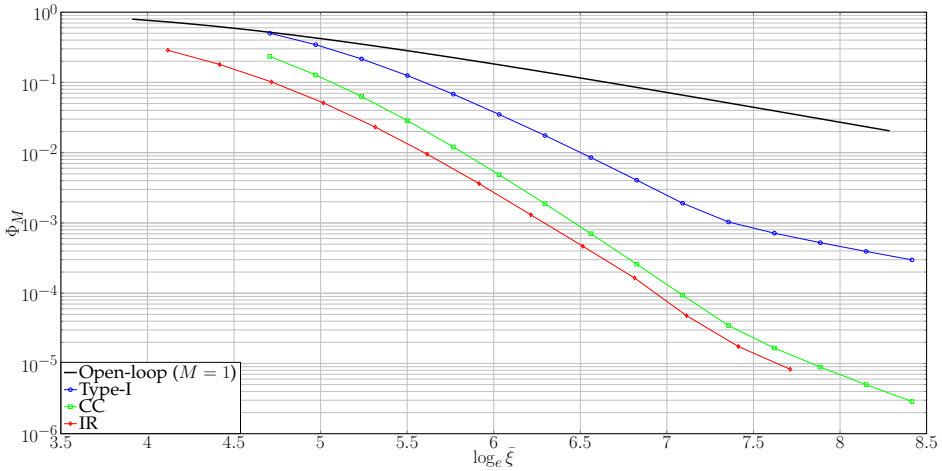

Figure 4.2. *Outage probability Φ_M vs average consumed energy $\bar{\xi}$ for $L = 50$. Note that $\bar{\xi}$ is represented in logarithmic scale.*

4.2.1 Outage Probability

Figs. 4.2 and 4.3 show the outage probability Φ_M vs the average consumed energy $\bar{\xi}$ for $L \in \{50, 200\}$.

The open-loop system, i.e., the system with no retransmissions ($M = 1$), is reported as a reference. The reader can infer that IR HARQ has the best performance in terms of outage probability, while CC HARQ behaves better than Type-I HARQ. Of course, all of the HARQ schemes outperform the open-loop system thanks to the retransmission process they employ. Note that the trend of the outage probability curves for $L = 200$ is the same as for $L = 50$, except for a shift in the average energy $\bar{\xi}$ of approximately 1.4 in the logarithmic scale, which is reasonable as $\log_e(200/50) = \log_e 4 \approx 1.4$.

Since the same consideration holds for the transmission powers $\{P_m\}_{m=1}^{M}$, in the fol-

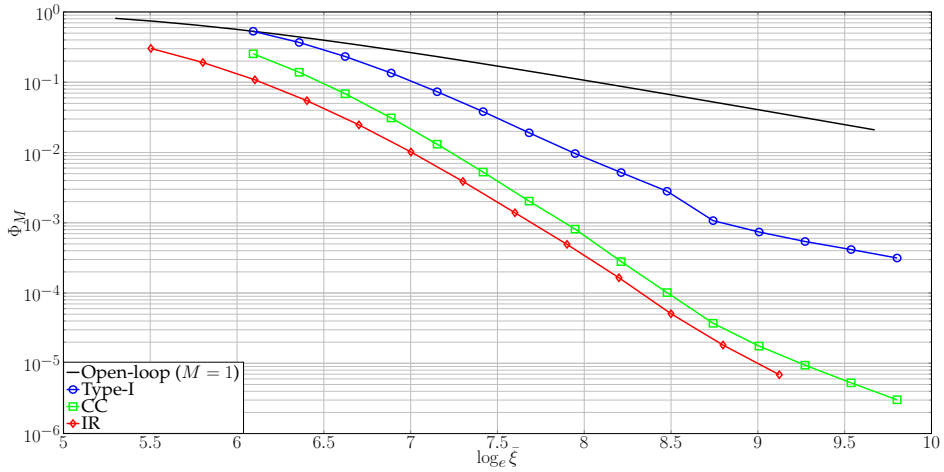

Figure 4.3. *Outage probability Φ_M vs average consumed energy $\bar{\xi}$ for $L = 200$. Note that $\bar{\xi}$ is represented in logarithmic scale.*

lowing we will analyze just the power allocation for $L = 50$.

4.2.2 Power Allocation

Fig. 4.4 shows the power allocation for the M transmission attempts vs the average consumed energy $\bar{\xi}$ for $L = 50$. It can be seen that, for both the Type-II HARQ processes, when the energy budget $\bar{\xi}$ is low, the best thing to do is to allocate more power on the first transmission attempt, i.e., $P_1 > P_2$. Then, when the available energy is higher, in particular if $\log_e \bar{\xi} \geq 5$ for CC HARQ and $\log_e \bar{\xi} \geq 5.3$ for IR HARQ, it is more convenient to allocate more power on the second transmission attempt, i.e., i.e., $P_1 < P_2$. For Type-I HARQ processes, instead, as already reported in [82], the optimal power allocation consists in always employing increasing transmission powers for successive transmission attempts. One can also infer that, as $\bar{\xi}$ grows, P_2 saturates to $P_{\max}$ and, therefore, P_1 increases, yielding a change of slope in the curves of both the power allocation and the outage probability. Note that, after the saturation, P_1 is the same for Type-I and CC HARQ processes.

A final observation can be made about the optimal transmission powers for IR HARQ processes. Indeed, they are always higher than those employed for the other two HARQ schemes. The reason for this is that the maximum amount of channel uses employed by IR HARQ is upper bounded by L, while for Type-I or CC HARQ the

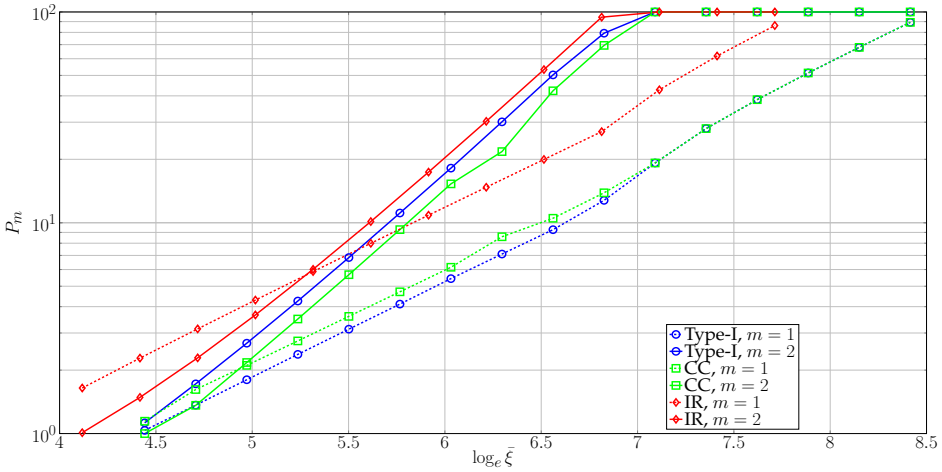

Figure 4.4. *Power allocation P_m vs average consumed energy $\bar{\xi}$ for $L = 50$. Note that $\bar{\xi}$ is represented in logarithmic scale.*

upper bound is $M \cdot L$. Since the energy budget $\bar{\xi}$ is the same for all the processes, IR HARQ uses higher transmission powers in all transmission attempts.

4.2.3 Delivery Delay

In Fig. 4.5 the average delivery delay τ of the three HARQ schemes is depicted for $L = 50$ channel uses.
The curves show that IR HARQ provides the best performance in terms of delay, employing a lower number of channel uses with respect to the other HARQ schemes. The trends of Type-I and CC HARQ, instead, are approximately the same. In particular, CC outperforms Type-I HARQ in the low energy budget regime, i.e., when the power allocations for the two schemes are different, while they perform exactly the same when the energy budget is high, i.e., when the power allocations are the same.

4.2.4 Energy Efficiency

Fig. 4.6 depicts the energy gain trend of Type-II HARQ processes with respect to Type-I HARQ, i.e., the energy gain provided by combining previously received packets before decoding. The reader can see that an energy gain from 40% to a con-

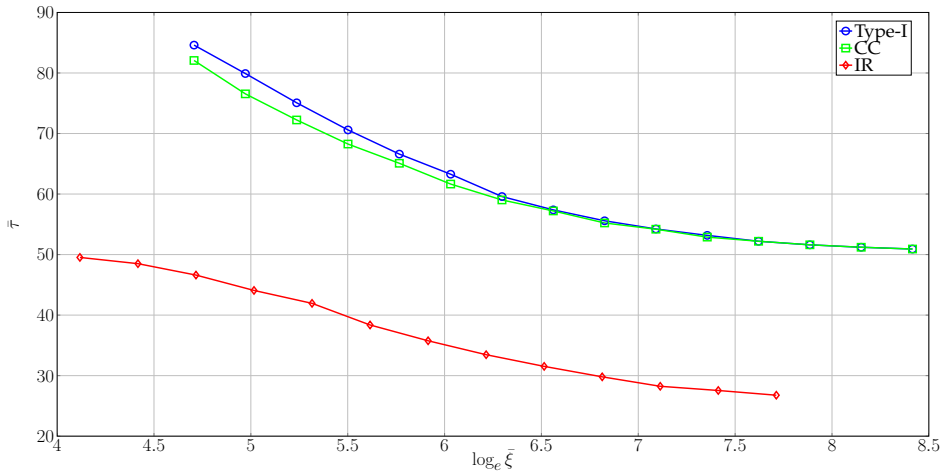

Figure 4.5. *Average number of channel uses $\bar{\tau}$ for Type-I, CC, and IR HARQ vs average consumed energy $\bar{\xi}$, when $L = 50$.*

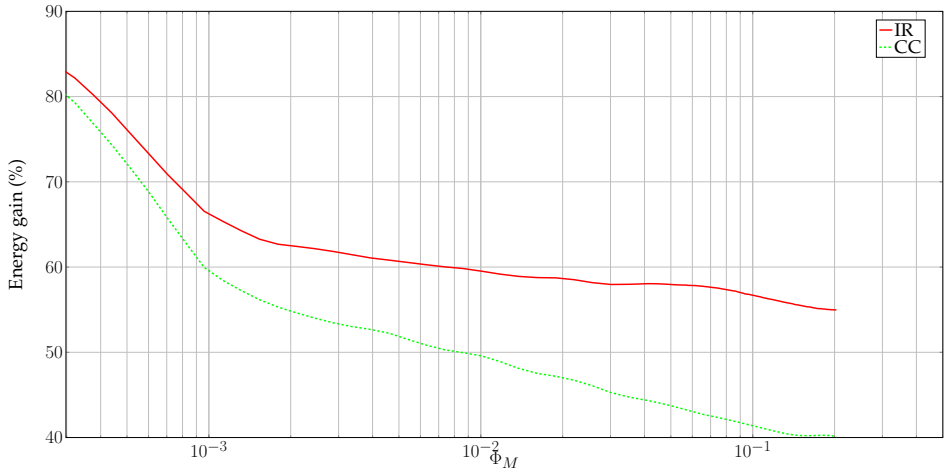

Figure 4.6. *Energy gap of CC HARQ and IR HARQ with respect to Type-I HARQ vs outage probability Φ_M for $L = 50$.*

siderable 80% can be obtained using Type-II HARQ. Moreover, it can be seen that the gain decreases as the outage probability increases, i.e., as the energy budget $\bar{\xi}$ is lower. Note, also, that when $P_2 = P_{\max}$, the change of slope in both the curves of outage probability and of the power allocation reflects in a change of slope of the energy gain curve, too, when $\Phi_M < 10^{-3}$.
Finally, we want to remark that the IR HARQ process always outperforms CC HARQ in terms of energy saving.

4.3 Final remarks

A novel comparison between Type-I, CC, and IR HARQ schemes has been provided in the context of energy-efficient finite block-length regime. This particular scenario is really timely, since low-complexity, energy-constrained devices will be employed to make new communication paradigms like IoT feasible and real. We have shown that combining previously received packets provides up to a considerable 80% energy saving.

Chapter 5

Conclusions

In this thesis we discussed several issues on machine type communications, spanning both theoretical aspects and practical implications.
After explaining the motivation for the need of a new mobile network generation, we presented current proposals for the future 5G networks, describing pros, cons and incompatibilities of these new technologies. We also introduced the concept of M2M communications, strictly correlated to the paradigm of the internet of things.
The dissertation then tackles two important practical applications of the M2M paradigm.
In chapter 2 we considered one of the most important applications of M2M, vehicular networks. In the first part of the chapter we highlighted the lack of resources for channel response estimation and tracking of the current IEEE 802.11p protocol. We introduced a new receiver scheme which improves the mechanism of pseudo-pilot tones construction by including the FEC decoder in the chain. We also showed how the receiver can benefit from the in-car electronic systems to enhance the receiving performances. The information about vehicle speed retrieved from in-car electronic units like speedometer or GPS receiver, is used to estimate the Doppler frequency. In combination with the estimated value of SNR, the receiver computes a "perceived SNR" value which takes into account averaging operations on subsequent channel response estimates. Finally it uses the $eSNR$ values computed for different averaging parameters to find the best trade-off among averaging for reducing noise and tracking channel changes to improve preciseness and robustness of the final channel response estimate. Simulations on packet error rate have been conducted in an Infrastructure-to-Vehicle scenario which is the most appropriate to

analyse long packet reception. Results show that both the improvements contribute to outperform other receiver schemes proposed in literature.
In the second part of the chapter we discussed limitations of the IEEE 802.11p protocol when operating in a multichannel environment. In particular we analysed channel occupancy detectors borrowed from the cognitive radio theory, and measured their performances in the vehicular environment. The analysis leads to the conclusion that the vehicular environment presents incompatible characteristics respect to the classical scenario of cellular networks, and, hence, schemes and protocols for these kind of networks perform extremely different when used in a vehicular ambient.
In chapter 3 we presented SiGLoWPAN, an IETF IPv6 / 6LoWPAN protocol stack implementation for low-energy devices. The protocol stack has been specifically designed for devices capable of communicating with more than one radio access technology. The innovative solutions for the memory management within the device and the packet handling procedures for datagram fragmentation and reconstruction, enable such resource-constrained devices to support IPv6 protocol over different link-layer protocols. The stack has been designed as a composition of simple modules, each in charge of a specific network function. The adopted lightweight design reveals its potential as big fragmented datagrams are delivered: in comparison with BLIP, a reference implementation for these protocols, the goodput of SiGLoWPANis increasingly higher as the datagram sizes grow.
In chapter 4 we analysed hybrid ARQ protocols using the novel theory on channel coding in finite block-length regime, more appropriate than the classical Shannon theory for the M2M scenario. We expressed in closed-form the formulae for the outage probability for the different protocols and we used them to formulate a power allocation optimization problem. In particular we found out the best power transmission allocation for the transmission attempts. The obtained results prove that the additional computation power requested to implement the combining techniques of HARQ protocols at the receiver, is paid back by the amount of energy that can be saved during the transmission.

List of Publications

The work presented in this thesis has appeared in the articles reported below.

Journal papers

[J1] **G. Ministeri**, L. Vangelista, "Channel Impulse Response Estimation in IEEE 802.11p via Data Fusion and MMSE Estimator", *International Journal of Vehicular Technology*, vol(2015), 2015.

Conference papers

[C1] A. Castellani, **G. Ministeri**, L.Rotoloni, L. Vangelista, M. Zorzi, "Interoperable and globally interconnected Smart Grid using IPv6 and 6LoWPAN", *IEEE International Conference on Communications 2012*

[C2] **G. Ministeri**, L. Vangelista, "On the performance of channel occupancy detectors for vehicular ad-hoc networks", *IEEE International Congress on Ultra Modern Telecommunications and Control Systems and Workshops 2013*

[C3] **G. Ministeri**, L. Vangelista, "Channel impulse response estimation in IEEE 802.11p via data fusion and group orthogonal matching pursuit", *IEEE International Symposium on a World of Wireless, Mobile and Multimedia Networks 2014*

[C4] M. Centenaro, **G. Ministeri**, L. Vangelista, "On Energy-Efficient HARQ Schemes for M2M Communication", *IEEE International Conference on Ubiquitous Wireless Broadband 2015*

Bibliography

[1] "Ericsson mobility report," Ericsson, Tech. Rep., June 2015.

[2] "Cisco visual networking index: Global mobile data traffic forecast update, 2014-2019," Cisco.com, White paper, February 3, 2015.

[3] G. Fettweis and S. Alamouti, "5g: Personal mobile internet beyond what cellular did to telephony," *Communications Magazine, IEEE*, vol. 52, no. 2, pp. 140–145, February 2014.

[4] J. Andrews, "Seven ways that hetnets are a cellular paradigm shift," *Communications Magazine, IEEE*, vol. 51, no. 3, pp. 136–144, March 2013.

[5] H. Ishii, Y. Kishiyama, and H. Takahashi, "A novel architecture for lte-b :c-plane/u-plane split and phantom cell concept," in *Globecom Workshops (GC Wkshps), 2012 IEEE*, Dec 2012, pp. 624–630.

[6] "C-ran: The road towards green ran," China Mobile Research Institute, White paper, October 2011.

[7] A. Osseiran, F. Boccardi, V. Braun, K. Kusume, P. Marsch, M. Maternia, O. Queseth, M. Schellmann, H. Schotten, H. Taoka, H. Tullberg, M. Uusitalo, B. Timus, and M. Fallgren, "Scenarios for 5g mobile and wireless communications: the vision of the metis project," *Communications Magazine, IEEE*, vol. 52, no. 5, pp. 26–35, May 2014.

[8] G. Wunder, M. Kasparick, S. ten Brink, F. Schaich, T. Wild, I. Gaspar, E. Ohlmer, S. Krone, N. Michailow, A. Navarro, G. Fettweis, D. Ktenas, V. Berg, M. Dryjanski, S. Pietrzyk, and B. Eged, "5gnow: Challenging the lte design paradigms of orthogonality and synchronicity," in *Vehicular Technology Conference (VTC Spring), 2013 IEEE 77th*, June 2013, pp. 1–5.

[9] "Ieee standard for information technology–telecommunications and information exchange between systems–local and metropolitan area networks–specific requirements-part 11: Wireless lan medium access control (mac) and physical layer (phy) specifications amendment 3: Enhancements for very high throughput in the 60 ghz band," *IEEE Std 802.11ad-2012 (Amendment to IEEE Std 802.11-2012, as amended by IEEE Std 802.11ae-2012 and IEEE Std 802.11aa-2012)*, pp. 1–628, Dec 2012.

[10] W. Hong, K.-H. Baek, Y. Lee, Y. Kim, and S.-T. Ko, "Study and prototyping of practically large-scale mmwave antenna systems for 5g cellular devices," *Communications Magazine, IEEE*, vol. 52, no. 9, pp. 63–69, September 2014.

[11] Z. Pi, F. Khan, and J. Zhang, "Techniques for millimeter wave mobile communication," Jul. 28 2011, uS Patent App. 12/916,019. [Online]. Available: http://www.google.com/patents/US20110182174

[12] V. Chandrasekhar, J. Andrews, and A. Gatherer, "Femtocell networks: a survey," *Communications Magazine, IEEE*, vol. 46, no. 9, pp. 59–67, September 2008.

[13] D. Ramasamy, R. Ganti, and U. Madhow, "On the capacity of picocellular networks," in *Information Theory Proceedings (ISIT), 2013 IEEE International Symposium on*, July 2013, pp. 241–245.

[14] F. Schaich, T. Wild, and Y. Chen, "Waveform contenders for 5g - suitability for short packet and low latency transmissions," in *Vehicular Technology Conference (VTC Spring), 2014 IEEE 79th*, May 2014, pp. 1–5.

[15] M. McGuire and M. Sima, "Discrete time faster-than-nyquist signalling," in *Global Telecommunications Conference (GLOBECOM 2010), 2010 IEEE*, Dec 2010, pp. 1–5.

[16] F. Rusek and J. Anderson, "Multistream faster than nyquist signaling," *Communications, IEEE Transactions on*, vol. 57, no. 5, pp. 1329–1340, May 2009.

[17] M. Bellanger, D. LeRuyet, D. Roviras, and M. Terr, "Fbmc physical layer : a primer," *www.ict-phydyas.org*.

[18] G. Wunder, M. Kasparick, T. Wild, F. Schaich, Y. Chen, M. Dryjanski, M. Buczkowski, S. Pietrzyk, N. Michailow, M. Matthe, I. Gaspar, L. Mendes, A. Festag, G. Fettweis, J.-B. Dore, N. Cassiau, D. Ktenas, V. Berg, B. Eged, and P. Vago, "5gnow: Intermediate frame structure and transceiver concepts," in *Globecom Workshops (GC Wkshps), 2014*, Dec 2014, pp. 565–570.

[19] J. Andrews, S. Buzzi, W. Choi, S. Hanly, A. Lozano, A. Soong, and J. Zhang, "What will 5g be?" *Selected Areas in Communications, IEEE Journal on*, vol. 32, no. 6, pp. 1065–1082, June 2014.

[20] E. Aryafar, M. A. Khojastepour, K. Sundaresan, S. Rangarajan, and M. Chiang, "Midu: Enabling mimo full duplex," in *Proceedings of the 18th Annual International Conference on Mobile Computing and Networking*, ser. Mobicom '12. New York, NY, USA: ACM, 2012, pp. 257–268. [Online]. Available: http://doi.acm.org/10.1145/2348543.2348576

[21] Y.-S. Choi and H. Shirani-Mehr, "Simultaneous transmission and reception: Algorithm, design and system level performance," *Wireless Communications, IEEE Transactions on*, vol. 12, no. 12, pp. 5992–6010, December 2013.

[22] S. Hong, J. Brand, J. Choi, M. Jain, J. Mehlman, S. Katti, and P. Levis, "Applications of self-interference cancellation in 5g and beyond," *Communications Magazine, IEEE*, vol. 52, no. 2, pp. 114–121, February 2014.

[23] S. Corroy, L. Falconetti, and R. Mathar, "Cell association in small heterogeneous networks: Downlink sum rate and min rate maximization," in *Wireless Communications and Networking Conference (WCNC), 2012 IEEE*, April 2012, pp. 888–892.

[24] Q. Ye, B. Rong, Y. Chen, M. Al-Shalash, C. Caramanis, and J. Andrews, "User association for load balancing in heterogeneous cellular networks," *Wireless Communications, IEEE Transactions on*, vol. 12, no. 6, pp. 2706–2716, June 2013.

[25] E. Aryafar, A. Keshavarz-Haddad, M. Wang, and M. Chiang, "Rat selection games in hetnets," in *INFOCOM, 2013 Proceedings IEEE*, April 2013, pp. 998–1006.

[26] P. Popovski, "Ultra-reliable communication in 5g wireless systems," in *5G for Ubiquitous Connectivity (5GU), 2014 1st International Conference on*, Nov 2014, pp. 146–151.

[27] "IEEE standard for information technology–telecommunications and information exchange between systems local and metropolitan area networks–specific requirements part 11: Wireless LAN medium access control (MAC) and physical layer (PHY) specifications," *IEEE P802.11-REVmb/D12, November 2011 (Revision of IEEE Std 802.11-2007, as amended by IEEEs 802.11k-2008, 802.11r-2008, 802.11y-2008, 802.11w-2009, 802.11n-2009, 802.11p-2010, 802.11z-2010, 802.11v-2011, 802.11u-2011, and 802.11s-2011)*, pp. 1 –2910, 29 2012.

[28] R. Stanica, E. Chaput, and A.-L. Beylot, "Properties of the mac layer in safety vehicular ad hoc networks," *Communications Magazine, IEEE*, vol. 50, no. 5, pp. 192 –200, may 2012.

[29] C. Han, M. Dianati, R. Tafazolli, R. Kernchen, and X. Shen, "Analytical study of the IEEE 802.11p mac sublayer in vehicular networks," *Intelligent Transportation Systems, IEEE Transactions on*, vol. 13, no. 2, pp. 873 –886, june 2012.

[30] A. Vinel, "3gpp lte versus ieee 802.11p/wave: Which technology is able to support cooperative vehicular safety applications?" *Wireless Communications Letters, IEEE*, vol. 1, no. 2, pp. 125–128, April 2012.

[31] J. Karedal, F. Tufvesson, N. Czink, A. Paier, C. Dumard, T. Zemen, C. Mecklenbrauker, and A. Molisch, "A geometry-based stochastic mimo model for vehicle-to-vehicle communications," *Wireless Communications, IEEE Transactions on*, vol. 8, no. 7, pp. 3646–3657, 2009.

[32] G. Acosta-Marum and D. Brunelli, "Six time- and frequency- selective empirical channel models for vehicular wireless LANs," *Vehicular Technology Magazine, IEEE*, vol. 2, no. 4, pp. 4–11, 2007.

[33] [Online]. Available: http://sourceforge.net/apps/mediawiki/physlayersim/

[34] [Online]. Available: http://itpp.sourceforge.net/current/

[35] H. Abdulhamid, K. E. Tepe, and E. Abdel-Raheem, "Performance of DSRC systems using conventional channel estimation at high velocities," *AEU - International Journal of Electronics and Communications*, vol. 61, no. 8, pp. 556 – 561, 2007. [Online]. Available: http://www.sciencedirect.com/science/article/pii/S1434841106001178

[36] M. Wellens, B. Westphal, and P. Mahonen, "Performance evaluation of ieee 802.11-based wlans in vehicular scenarios," in *Vehicular Technology Conference, 2007. VTC2007-Spring. IEEE 65th*, April 2007, pp. 1167–1171.

[37] N. Benvenuto and G. Cherubini, *Algorithms for Communications Systems and their Applications*. John Wiley & Sons, 2002, ch. 9.

[38] S. I. Kim, H. seo Oh, and H.-K. Choi, "Mid-amble aided OFDM performance analysis in high mobility vehicular channel," in *Intelligent Vehicles Symposium, 2008 IEEE*, June 2008, pp. 751–754.

[39] Y. Zhang, I. L. Tan, C. Chun, K. Laberteaux, and A. Bahai, "A differential ofdm approach to coherence time mitigation in dsrc," in *Proceedings of the Fifth ACM International Workshop on VehiculAr Inter-NETworking*, ser. VANET '08. New York, NY, USA: ACM, 2008, pp. 1–6. [Online]. Available: http://doi.acm.org/10.1145/1410043.1410045

[40] T. Zemen, L. Bernado, N. Czink, and A. Molisch, "Iterative time-variant channel estimation for 802.11p using generalized discrete prolate spheroidal sequences," *Vehicular Technology, IEEE Transactions on*, vol. 61, no. 3, pp. 1222–1233, 2012.

[41] L. Bahl, J. Cocke, F. Jelinek, and J. Raviv, "Optimal decoding of linear codes for minimizing symbol error rate (corresp.)," *Information Theory, IEEE Transactions on*, vol. 20, no. 2, pp. 284–287, Mar 1974.

[42] A. Bourdoux, H. Cappelle, and A. Dejonghe, "Channel tracking for fast time-varying channels in IEEE 802.11p systems," in *Global Telecommunications Conference (GLOBECOM 2011), 2011 IEEE*, 2011, pp. 1–6.

[43] J. Fernandez, K. Borries, L. Cheng, B. Kumar, D. Stancil, and F. Bai, "Performance of the 802.11p physical layer in vehicle-to-vehicle environments," *Vehicular Technology, IEEE Transactions on*, vol. 61, no. 1, pp. 3–14, 2012.

[44] Z. Zhao, X. Cheng, M. Wen, B. Jiao, and C.-X. Wang, "Channel estimation schemes for IEEE 802.11p standard," *Intelligent Transportation Systems Magazine, IEEE*, vol. 5, no. 4, pp. 38–49, 2013.

[45] C.-J. Wu and D. Lin, "Sparse channel estimation for ofdm transmission based on representative subspace fitting," in *Vehicular Technology Conference, 2005. VTC 2005-Spring. 2005 IEEE 61st*, vol. 1, May 2005, pp. 495–499 Vol. 1.

[46] B. Yang, K. Letaief, R. Cheng, and Z. Cao, "Channel estimation for ofdm transmission in multipath fading channels based on parametric channel modeling," *Communications, IEEE Transactions on*, vol. 49, no. 3, pp. 467–479, Mar 2001.

[47] A. Molisch, F. Tufvesson, J. Karedal, and C. Mecklenbrauker, "A survey on vehicle-to-vehicle propagation channels," *Wireless Communications, IEEE*, vol. 16, no. 6, pp. 12–22, 2009.

[48] T. Abbas, L. Bernado, A. Thiel, C. Mecklenbrauker, and F. Tufvesson, "Radio channel properties for vehicular communication: Merging lanes versus urban intersections," *Vehicular Technology Magazine, IEEE*, vol. 8, no. 4, pp. 27–34, 2013.

[49] T. Hastie, R. Tibshirani, and J. Friedman, *The Elements of Statistical Learning*, ser. Springer Series in Statistics. New York, NY, USA: Springer New York Inc., 2001.

[50] A. Molisch, *Wireless Communications*. Wiley-IEEE Press, 2005.

[51] M. Siti, A. Agnoletto, and A. Assalini, "Doppler spread estimation and channel update period tuning in OFDM-based vehicular communication systems," in *Vehicular Technology Conference (VTC Spring), 2011 IEEE 73rd*, 2011, pp. 1–5.

[52] G. Ren, H. Zhang, and Y. Chang, "SNR estimation algorithm based on the preamble for OFDM systems in frequency selective channels," *Communications, IEEE Transactions on*, vol. 57, no. 8, pp. 2230–2234, Aug 2009.

[53] A. Abdi, J. Barger, and M. Kaveh, "A parametric model for the distribution of the angle of arrival and the associated correlation function and power spectrum at the mobile station," *Vehicular Technology, IEEE Transactions on*, vol. 51, no. 3, pp. 425–434, May 2002.

[54] A. Doukas and G. Kalivas, "Rician k factor estimation for wireless communication systems," in *Wireless and Mobile Communications, 2006. ICWMC '06. International Conference on*, July 2006, pp. 69–69.

[55] G. Azemi, B. Senadji, and B. Boashash, "Ricean k-factor estimation in mobile communication systems," *Communications Letters, IEEE*, vol. 8, no. 10, pp. 617–619, Oct 2004.

[56] M. van Eenennaam, A. van de Venis, and G. Karagiannis, "Impact of IEEE 1609.4 channel switching on the IEEE 802.11p beaconing performance," in *Wireless Days (WD), 2012 IFIP*, 2012, pp. 1–8.

[57] D. Borota, G. Ivkovic, R. Vuyyuru, O. Altintas, I. Seskar, and P. Spasojevic, "On the delay to reliably detect channel availability in cooperative vehicular environments," pp. 1 –5, may 2011.

[58] H. Urkowitz, "Energy detection of unknown deterministic signals," *Proceedings of the IEEE*, vol. 55, no. 4, pp. 523 – 531, april 1967.

[59] E. Axell and E. Larsson, "Optimal and sub-optimal spectrum sensing of OFDM signals in known and unknown noise variance," *Selected Areas in Communications, IEEE Journal on*, vol. 29, no. 2, pp. 290 –304, february 2011.

[60] S. Chaudhari, V. Koivunen, and H. Poor, "Autocorrelation-based decentralized sequential detection of OFDM signals in cognitive radios," *Signal Processing, IEEE Transactions on*, vol. 57, no. 7, pp. 2690–2700, 2009.

[61] L. Lai, Y. Fan, and H. Poor, "Quickest detection in cognitive radio: A sequential change detection framework," in *Global Telecommunications Conference, 2008. IEEE GLOBECOM 2008. IEEE*, 2008, pp. 1–5.

[62] A. Wald, *Sequential Analysis*, 1st ed. John Wiley and Sons, 1947.

[63] I. Sen and D. Matolak, "Vehicle - vehicle channel models for the 5-ghz band," *Intelligent Transportation Systems, IEEE Transactions on*, vol. 9, no. 2, pp. 235–245, 2008.

[64] J. Zhang, L. Shan, H. Hu, and Y. Yang, "Mobile cellular networks and wireless sensor networks: toward convergence," *Communications Magazine, IEEE*, vol. 50, no. 3, pp. 164–169, March 2012.

[65] C. Hauser, D. Bakken, and A. Bose, "A failure to communicate: next generation communication requirements, technologies, and architecture for the electric power grid," *IEEE Power Energy Mag.*, vol. 3, no. 2, pp. 47–55, 2005.

[66] IETF 6LoWPAN Working Group. [Online]. Available: http://tools.ietf.org/wg/6lowpan

[67] P. Levis, S. Madden, D. Gay, J. Polastre, R. Szewczyk, A. Woo, E. Brewer, and D. Culler, "The emergence of networking abstractions and techniques in TinyOS," in *Proc. of the NSDI*. Berkeley, CA, USA: USENIX Association, 2004, pp. 1–1. [Online]. Available: http://dl.acm.org/citation.cfm?id=1251175.1251176

[68] A. P. Castellani, P. Casari, and M. Zorzi, "TinyNET–a tiny network framework for TinyOS: description, implementation, and experimentation," *Wireless Communications and Mobile Computing*, vol. 10, no. 1, pp. 101–114, 2010.

[69] A. P. Castellani, N. Bui, P. Casari, M. Rossi, Z. Shelby, and M. Zorzi, "Architecture and Protocols for the Internet of Things: A Case Study," in *IEEE WoT*, Mannheim, Germany, Mar-Apr 2010.

[70] A. P. Castellani, M. Gheda, N. Bui, M. Rossi, and M. Zorzi, "Web services for the Internet of Things through CoAP and EXI," in *IEEE ICC RWFI Workshop*, Kyoto, Japan, Jun. 2011.

[71] U. Sarwar, G. S. Rao, Z. Suryady, and R. Khoshdelniat, "A comparative study on available IPv6 platforms for wireless sensor network," World Academy of Science, Engineering and Technology, 2010.

[72] T. Winter, P. Thubert, A. Brandt, T. Clausen, J. Hui, R. Kelsey, P. Levis, K. Pister, R. Struik, and J. Vasseur, "RPL: IPv6 Routing Protocol for Low power and Lossy Networks," IETF Internet Draft draft-ietf-roll-rpl-12, 2010. [Online]. Available: https://datatracker.ietf.org/doc/draft-ietf-roll-rpl/

[73] J. Nieminen, B. Patil, T. Savolainen, M. Isomaki, Z. Shelby, and C. Gomez, "Transmission of IPv6 Packets over Bluetooth Low Energy," IETF Internet Draft draft-ietf-6lowpan-btle, 2011. [Online]. Available: http://tools.ietf.org/html/draft-ietf-6lowpan-btle-03

[74] I. Team. [Online]. Available: http://iperf.sourceforge.net/

[75] CrossBow, "TelosB Mote Platform." [Online]. Available: http://www.xbow.com/Products/Product_pdf_files/Wireless_pdf/TelosB_Datasheet.pdf

[76] J. F. Cheng, "Coding Performance of Hybrid ARQ Schemes," *IEEE Transactions on Communications*, vol. 54, no. 6, Jun. 2006.

[77] ——, "On the coding gain of incremental redundancy over chase combining," in *IEEE Global Telecommunications Conference (GLOBECOM)*, Dec. 2003, pp. 107–112, vol. 1.

[78] G. Caire, G. Taricco, and E. Biglieri, "Optimum power control over fading channels," *IEEE Transactions on Information Theory*, vol. 45, no. 5, pp. 1468–1489, Jul. 1999.

[79] G. Caire and D. Tuninetti, "The throughput of hybrid-ARQ protocols for the Gaussian collision channel," *IEEE Transactions on Information Theory*, vol. 47, no. 5, pp. 1971–1988, Jul. 2001.

[80] Y. Polyanskiy, H. Poor, and S. Verdu, "Channel Coding Rate in the Finite Blocklength Regime," *IEEE Transactions on Information Theory*, vol. 56, no. 5, pp. 2307–2359, May 2010.

[81] C. Shannon, "A Mathematical Theory of Computation," *The Bell System Technical Journal*, vol. 27, 1948.

[82] B. Makki, T. Svensson, and M. Zorzi, "Green communication via Type-I ARQ: Finite block-length analysis," in *IEEE Global Communications Conference (GLOBECOM)*, Dec. 2014, pp. 2673–2677.

[83] ——, "Finite Block-Length Analysis of the Incremental Redundancy HARQ," *IEEE Wireless Communications Letters*, vol. 3, no. 5, pp. 529–532, Oct. 2014.

[84] A. Goldsmith, *Wireless Communications*. Cambridge University Press, 2005.

[85] Y. Polyanskiy, H. Poor, and S. Verdu, "Dispersion of Gaussian channels," in *IEEE International Symposium on Information Theory*, Jun. 2009, pp. 2204–2208.

[86] Neul, "Clean Slate Retransmission Scheme," Technical Report GP-140831, 3GPP TSG GERAN#64, Nov. 2014.